ESTIMATION OF ELECTROMECHANICAL OSCILLATIONS IN THE NORDIC POWER SYSTEM USING SYNCHROPHASOR MEASUREMENT DATA

July, 2011

SEBASTIAN BENGTSSON

KTH Electrical Engineering

Master's Degree Project
Stockholm, Sweden 2011

XR-EE-ES
2011:015

ESTIMATION OF ELECTROMECHANICAL OSCILLATIONS IN THE NORDIC POWER SYSTEM USING SYNCHROPHASOR MEASUREMENT DATA

— Diploma Thesis —

Sebastian Bengtsson

Electrical Power Systems Division
School of Electrical Engineering, KTH Royal Institute of Technology, Sweden

Supervisor
Dr. Luigi Vanfretti
KTH Stockholm

Stockholm, July, 2011

Abstract

Unstable electromechanical dynamics, or electromechanical modes, may cause large amplitude oscillations that may lead to system break-ups or partial blackouts. Thus, the monitoring and study of these modes are of prominent importance and can be of great help for system operators and planning engineers.

In this thesis ambient data analysis has been applied on both simulated and synchronized phasor data from Phasor Measurement Units (PMUs) installed at the distribution network of the Nordic power system at Tampere, Lund and Luleå to estimate frequencies and damping ratios of electromechanical modes in the systems. Different spectral estimators (Yule-Walker, Multitaper and Welch) have been used and their performance has been evaluated. Damping estimates were obtained using an autoregressive Yule-Walker model and the half-power point method. Emphasis on general handling and preprocessing of PMU data is made throughout the thesis.

The performed analysis indicates that within the measurement locations available, two main inter-area modes in the Nordic power system can be estimated at approximately 0.4 Hz and 0.5 Hz. In addition relevant system dynamics in the frequency range of 0.6-1.0 Hz can also be observed.

Ambient data analysis techniques have great potential for monitoring electromechanical oscillations in power systems. However, there are issues related to data quality that need to be systematically addressed, especially when it comes to calculating accurate damping estimates, in the presence of undamped low amplitude sinusoids and forced oscillations.

Sammanfattning

Instabil elektromekanisk dynamik, eller elektromekaniska moder, kan orsaka oscillationer av hög amplitud som kan leda till sammanbrott av ett elkraftssystem eller till lokala strömavbrott. Således, övervakning och studie av dessa moder är av stor betydelse och kan vara till stor hjälp för systemoperatörer och planeringsingenjörer.

I detta examensarbete har ambient dataanalys använts både på simulerad och synkroniserad fasvektordata från Phasor Measurement Units (PMUs) installerade i det Nordiska elkraftsystemets distributionsnät vid Tammerfors, Lund och Luleå för att uppskatta frekvenser och dämpning av de elektromekaniska moderna i systemet. Olika spektrala estimatorer (Yule-Walker, Multitaper och Welch) har använts och deras resultat har utvärderats. Uppskattningar av dämpningen har erhållits med hjälp av den autoregressiva Yule-Walker modellen och Half-Power Point-metoden. Stor vikt har lagts på allmän hantering och förbehandling av PMU data genom hela examensarbetet.

Den utförda analysen indikerar att vid de tillgängliga mätstationerna kan två mellan-områdes moder i det Nordiska elkraftsystemet uppskattas till cirka 0.4 Hz och 0.5 Hz. Dessutom kan relevant systemdynamik i frekvensområdet 0.6-1.0 Hz observeras.

Ambienta dataanalys tekniker har stor potential för övervakning av elektromekaniska oscillationer i elkraftsystem. Det finns dock problem som rör datakvalitet som systematiskt måste tas om hand, särskilt när det gäller att beräkna precisa uppskattningar av dämpningen, i närvaro av odämpade låg amplituda sinusoider och påtvingade oscillationer.

Contents

Notations

Chapter 1

x	State vector
f, g, h	Nonlinear functions
x_d	Vector of dynamic variables
x_a	Vector of algebraic variables
u	Input vector
y	Output vector
A_{dae}, B_{dae}, C_{dae} D_{dae}	Partial differentiation matrices
A	State matrix
B	Input matrix
C	Output matrix
D	Feedfoward matrix
λ	Eigenvalue/Pole
I	Unit matrix
σ	Damping
ω	Mode frequency
f	Frequency
ζ	Damping ratio
X_r	Phasor (real part)
X_i	Phasor (imaginary part)
X_m	Peak magnitude
θ	Phase angle
A	Amplitude
t	Time
q	Random vector
u_E	Input signal
s'	Unknown topology change
s	Known topology change
$y(t)$	Output
μ	Measurement noise

Chapter 3

f, t	Interpolated sample
f_0, t_0	Preceding sample
f_1, t_1	Following sample

Chapter 4

$u(t)$	Input
$y(t)$	Output
$S_{uu}(\omega)$	Input spectral density matrix
$S_{yy}(\omega)$	Output spectral density matrix
$H(\omega)$	Frequency response function
A	Residue
λ	Pole
ω	Mode frequency
$a_1, a_2, .., a_k$	Power spectral density parameters
f	Frequency
$S(f)$	Power spectral density
$X_1, X_2, .., X_N$	Observations
$\hat{S}(f)$	Power spectral density estimate
$\hat{a}_1, \hat{a}_2, .., \hat{a}_k$	Parameter estimates
p	Autoregressive model order
Y_t	Zero mean stationary process
$\phi_{1,p}, \phi_{2,p}, .., \phi_{p,p}$	Yule-Walker spectral estimator coefficients
σ_p	Innovation variance
ϵ_t	White noise process with zero mean and variance σ_p^2
E	Expectation
s_k	Autocovariance sequence
$\hat{s}_k$	Autocovariance sequence estimate
$\hat{\phi}_p$	Yule-Walker spectral estimator coefficient estimates
$\hat{\sigma}_p$	Innovation variance estimate
τ	Lag value
N_B	Number of blocks
N_B	Number of samples per block
$F(f)$	Fejèrs kernel
h_t	Data taper
$\phi_{k,k}$	Partial autocorrelation coefficients
$\hat{\phi}_{k,k}$	Partial autocorrelation coefficients estimate

Chapter 5

λ	Eigenvalue/Pole
σ	Damping
ω	Mode frequency
ζ	Damping ratio
$\hat{y}(t)$	Transient estimate
t	Time
R	Residue
$H(s)$	Transfer function
σ_p	Innovation variance
$\phi_{1,p}, \phi_{2,p}, .., \phi_{p,p}$	Yule-Walker spectral estimator coefficients
f	Frequency
$H(\omega)$	Frequency response

Chapter 1

Introduction

1.1 Background

Interconnected electrical power systems are very complex dynamical systems. They consist of a wide variety of components connected together to form a system capable of generating, transmitting and distributing electrical energy over large areas. Because of the interaction of all these components there are many different types of dynamics in the system [1]. The system's electromechanical dynamics are associated with generator rotor masses swinging relative to each other [2] and are of great importance when it comes to stability. Unstable electromechanical dynamics may cause large amplitude oscillations that may lead to partial system break-ups or blackouts [3].

These electromechanical dynamics, or electromechanical modes, can be described by their frequency and damping ratio. Thus, the monitoring and study of these mode properties offer considerable insight into the small-signal stability properties of a power system [4] and can be of great help for system operators and planning engineers.

Data for analysis and system monitoring can be obtained from Wide-Area Measurement Systems (WAMS). However, the most commonly used techniques for estimation of modal properties of the electromechanical modes depend on the existence of transient data and can not be used for continuous monitoring. This thesis investigates the use of spectral analysis techniques to estimate frequencies and damping ratios of the electromechanical modes of a system under ambient conditions.

1.2 Power System Electromechanical Modes

Power systems contain many modes of oscillation, most of these are due to generator rotor masses swinging relative to each other. A power system having multiple machines will act like a set of masses interconnected by a network of springs and will exhibit multiple modes of oscillation [2].

The dynamics of such a system can be described by a nonlinear model consisting of a set of differential-algebraic equations [1]

$$\dot{x} = f(x_d, x_a, u) \tag{1.1}$$

$$0 = g(x_d, x_a, u) \tag{1.2}$$

$$y = h(x_d, x_a, u) \tag{1.3}$$

here x_d and x_a are the vectors of the dynamic and algebraic variables while u and y are the input and output vectors.

For small deviations from a stationary operation point $y_0 = h(x_{d0}, x_{a0}, u_0)$ a linear model can be approximated with

$$E_{dae}\frac{d}{dt}\begin{bmatrix} \Delta x_d \\ \Delta x_a \end{bmatrix} = A_{dae}\begin{bmatrix} \Delta x_d \\ \Delta x_a \end{bmatrix} + B_{dae}\Delta u \tag{1.4}$$

$$\Delta y = C_{dae}\begin{bmatrix} \Delta x_d \\ \Delta x_a \end{bmatrix} + D_{dae}\Delta u \tag{1.5}$$

where A_{dae}, B_{dae}, C_{dae} and D_{dae} are partial differentiation matrices.

$$A_{dae} = \begin{bmatrix} \frac{\partial f}{\partial x_d} & \frac{\partial f}{\partial x_a} \\ \frac{\partial g}{\partial x_d} & \frac{\partial g}{\partial x_a} \end{bmatrix} = \begin{bmatrix} A_{11} & A_{12} \\ A_{21} & A_{22} \end{bmatrix} \qquad B_{dae} = \begin{bmatrix} \frac{\partial f}{\partial u} \\ \frac{\partial g}{\partial u} \end{bmatrix} = \begin{bmatrix} B_1 \\ B_2 \end{bmatrix}$$

$$C_{dae} = \begin{bmatrix} \frac{\partial h}{\partial x_d} & \frac{\partial h}{\partial x_a} \end{bmatrix} = \begin{bmatrix} C_1 & C_2 \end{bmatrix} \qquad D_{dae} = \begin{bmatrix} \frac{\partial h}{\partial u} \end{bmatrix} = \begin{bmatrix} D_1 \end{bmatrix}$$

$$E_{dae} = \begin{bmatrix} I & 0 \\ 0 & 0 \end{bmatrix}$$

The algebraic variables x_a can be eliminated with

$$x_a = -A_{22}^{-1}(A_{21}x_d + B_2 u) \tag{1.6}$$

$$A = A_{11} - A_{12}A_{22}^{-1}A_{21} \quad B = B_1 - A_{12}A_{22}^{-1}B_2$$

$$C = C_1 - C_2A_{22}^{-1}A_{21} \quad D = D_1 - C_2A_{22}^{-1}B_2$$

Yielding the following linear model

$$\dot{x}(t) = Ax(t) + Bu(t) \tag{1.7}$$

$$y(t) = Cx(t) + Du(t) \tag{1.8}$$

here x, u and y are the state, input and output vectors. And A, B, C and D are the state, input, output and feedforward matrices.

The eigenvalues, λ, of this system are given by the state matrix A

$$det(A - \lambda I) = 0 \tag{1.9}$$

each of these eigenvalues correspond to a mode, which can be described by

$$\lambda_i = \sigma_i \pm j\omega_i \tag{1.10}$$

A mode frequency is given by

$$f_i = \frac{\omega_i}{2\pi} \tag{1.11}$$

and the damping ratio, or rate of decay, of an oscillatory mode can be computed

$$\zeta_i = \frac{-\sigma_i}{\sqrt{\sigma_i^2 + \omega_i^2}} \tag{1.12}$$

There are a few different types of power system modes described in [2], however, in this thesis only two of these will be of concern

- Local modes - associated with generators oscillating in a specific part of the power system, and with typical frequencies in the 1-2Hz range.
- Inter-area modes - associated with generators in one part of the system oscillating against generators in other parts of the system. The natural frequencies of these modes are in the 0.1-1Hz range, exhibiting far more complex characteristics than local modes.

1.3 Phasor Measurement Units (PMUs)

PMUs are used to measures phasors at specific locations in power systems, phasors are complex numbers which can be used to describe magnitude and phase angle of the positive sequence component derived from the three phase waveforms in an AC power system. The key idea is to define the voltage or current with respect to its cosine, the phase is then the angular difference between the observed value and the peak value, illustrated in Fig.1.1.

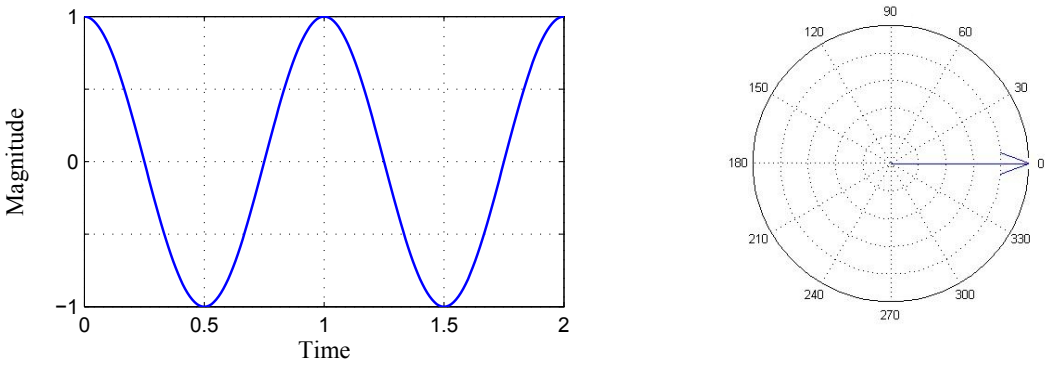

(a) (b)

Figure 1.1: (a) Cosine (b) Phasor representation of the cosine at t=0, phase angle $0°$ and magnitude 1.

Voltage and current can thus be described using complex numbers - phasor representation

$$X_r + jX_i = (X_m/\sqrt{2})e^{i\theta} \tag{1.13}$$

where X_m is the peak magnitude and θ is the phase angle. This representation compared to the time-domain representation

$$\mathrm{A}\cos(\omega t + \theta) \tag{1.14}$$

have the benefit that the time dependent frequency factor can be factored out, hence the use of this phasor notation considerably simplifies not only the mathematics but also the amount of electronics and processing power required [5].

The measurements are time-stamped and synchronized using a global positioning system (GPS). A pulse is sent from the GPS (typically one per second) to PMUs located in different areas of the system, this pulse is then used as a reference for synchronization, synchronized measurements are therefore called synchrophasors.

In Fig.1.2 a conceptual diagram of a phasor measurement unit is shown.

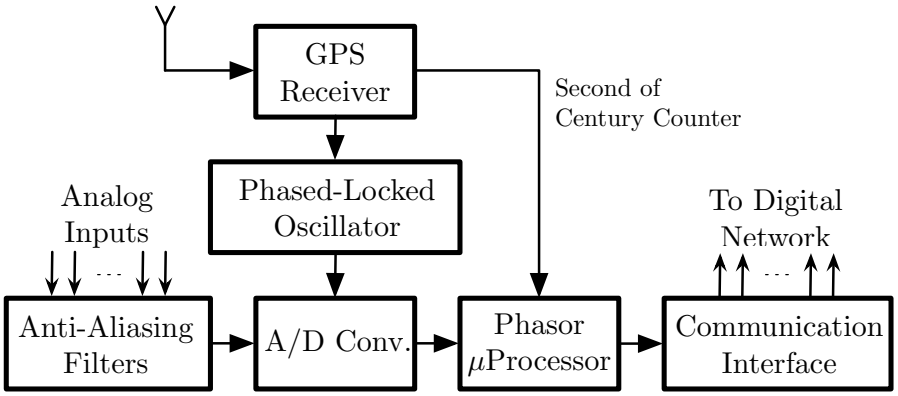

Figure 1.2: Conceptual diagram of a phasor measurement unit [6].

The following tasks are performed by the PMU:

- Analog inputs are filtered with an anti-alias filter.
- The input is sampled at the A/D converter. A digital decimation filter reduces the sampling rate, the sampler is phase-locked with the GPS pulses.
- The μ-processor estimates the frequency from the estimated data and the GPS time-tags and reports the estimates and measurements at a rate of 10 to 60 samples per second.
- The communication interface transfers the GPS-timestamped samples to a digital communication network.

In this master thesis voltage magnitude and voltage phase angle are measured and the frequency derived 50 times per second in three different PMUs located in Lund (LTH), Luleå (LTU) and Tampere, as shown in Fig.1.3.

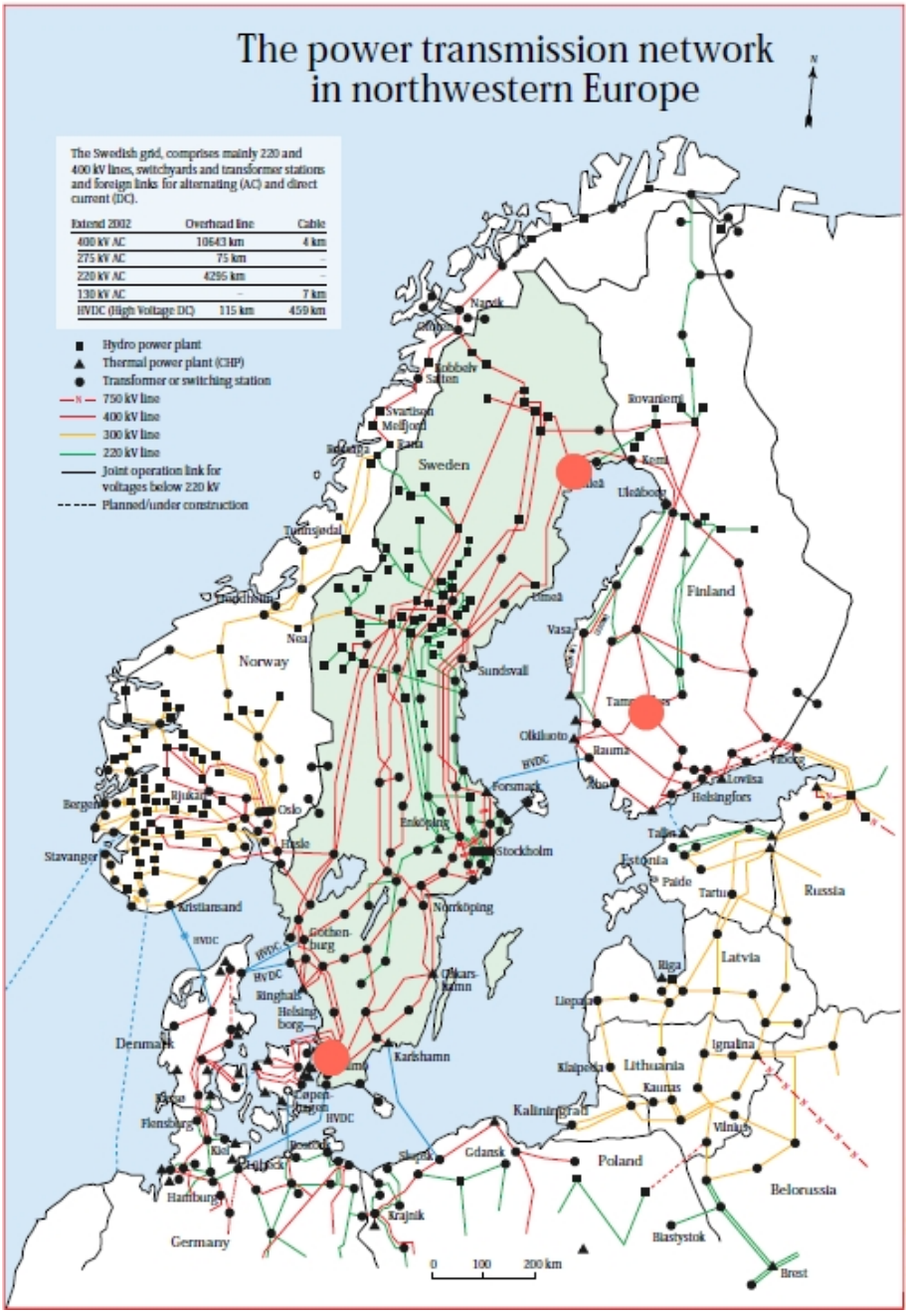

Figure 1.3: The Nordic power system - location of the PMUs marked with red dots [7].

1.4 Wide-Area Measurement Systems (WAMS)

In order to ensure the stability of a power system, and to be able to determine appropriate control actions, system operators need to have real-time measurements from many locations of the system available to them. To be able to provide this information PMUs can be installed at important locations, such as power stations, transformers and substations creating a wide-area measurement system (WAMS). In figure Fig1.4 a system utilizing PMUs to provide the system operator with information is depicted.

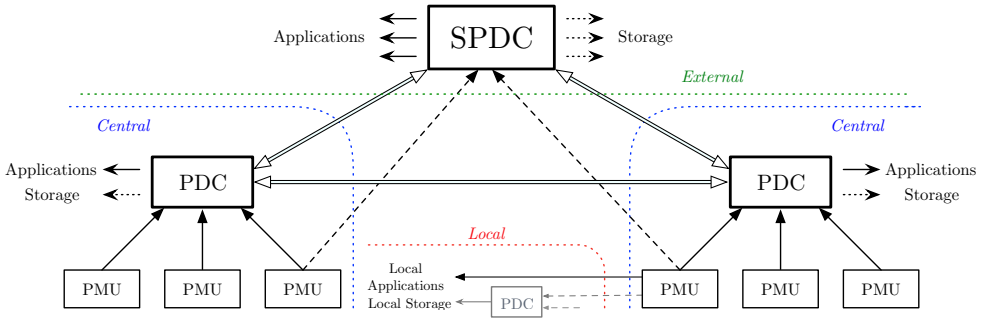

Figure 1.4: Generic architecture of a wide area monitoring and control system[6].

Phasor data concentrators (PDCs) and super phasor data concentrators (SPDCs) are computer systems receiving, processing, and sending out results to applications and storage, or signals for control. PMU data can be stored and accessed at a local, central or external levels. At local levels a PDC may not be necessary, but at central level when there are several units, data may not arrive simultaneously and therefore a PDC is required so that the data is time-aligned and concentrated.

1.5 Data Types

The measurements collected by PMUs may contain data sequences with different characteristics, they can be of either ambient (which is the data type used in this thesis), transient or probing data [3]. To show how the types of data that can arise in the system, the model in Fig.1.5 can be used

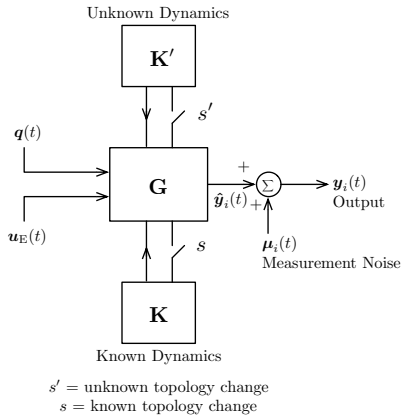

Figure 1.5: Block representation of a power system [8].

here q is an hypothetical random vector perturbing the system and u_E is a input signal.

By using u_E to inject known low level inputs into the system probing data can be obtained. Ambient data is the result of random low-amplitude variations at q while transient data, which is in general much larger in amplitude, are caused by a sudden switch at s or s', or a sudden step or pulse input at u_E. Fig.1.6 shows a transient surrounded by ambient data.

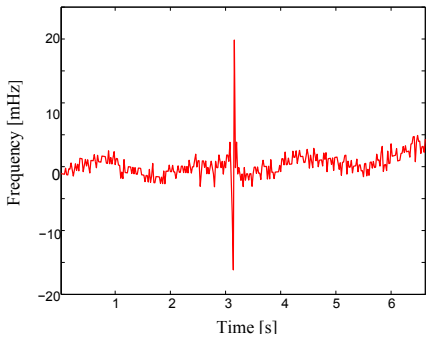

Figure 1.6: Measurements from Tampere's PMU show a transient surrounded by ambient data.

Chapter 2

Data Handling

To be able to efficiently process and analyze the massive amounts of data obtained, important considerations have to be taken for data storage and handling.

2.1 openPDC and openHistorian

The phasor data used for this thesis was obtained from PMUs installed in the Nordic grid (see Fig.1.3) which are stored on a server using the openPDC [9] and the openHistorian [10] open source software from Grid Protection Alliance. The open source phasor data concentrator, openPDC, is a software system that can receive streamed time-series data, in real-time, from several sources, the measurements are time-aligned and sorted. The measurements are then stored in the openHistorian software which archives and stores data locally on a server in flat binary archive files. openHistorian does not use a relational database management system, such as MySQL, because it would be inefficient for this large amount of data [11].

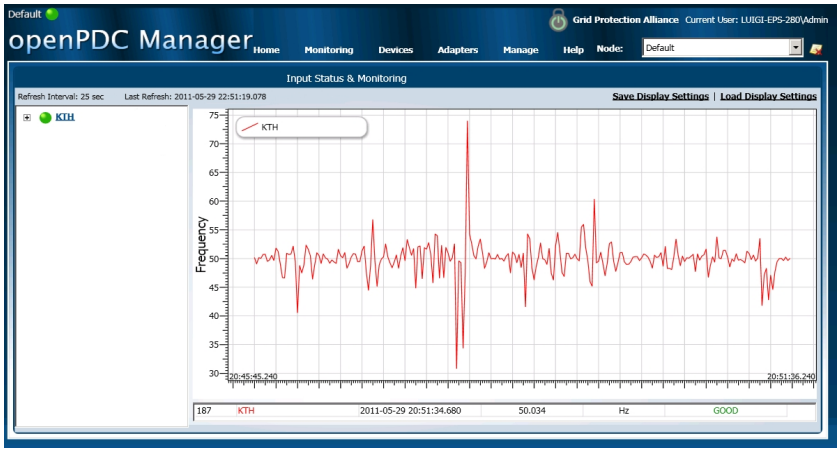

Figure 2.1: Screenshot of the openPDC Manager installed at KTH, showing estimated frequency, at a PMU in KTH.

2.2 Historian Playback Utility

Data is extracted from the openHistorian archive with the Historian Playback Utility (HPU). This program allows you to choose the time interval, data type and device from which you want to extract data. The format in which data is going to be extracted needs to be specified in the HPU, the following format specification was used:

$\{0 : I\}; \{1 : T\}; \{2 : V\};$

There are many file types to which the data can be extracted to. Preference was given to character files, in this case the delimiter "; " acts as a separator between the identifier, time stamp and value. The different value types and their identifiers are shown in the table below.

	TAMPERE	LTH	LTU
Frequency	110	105	100
Voltage Angle	113	108	103
Voltage Magnitude	114	109	104

Table 2.1: The different value types, PMU and their identifiers

Data extraction from the openHistorian into .csv files can be computationally intensive due to the massive amount of data stored and the extraction mechanisms used. To avoid putting unnecessary strains on the server, and also to avoid possible software out of memory errors, the files are extracted 12 hours and one device at a time. The total database size for three days is approximately 3600MB.

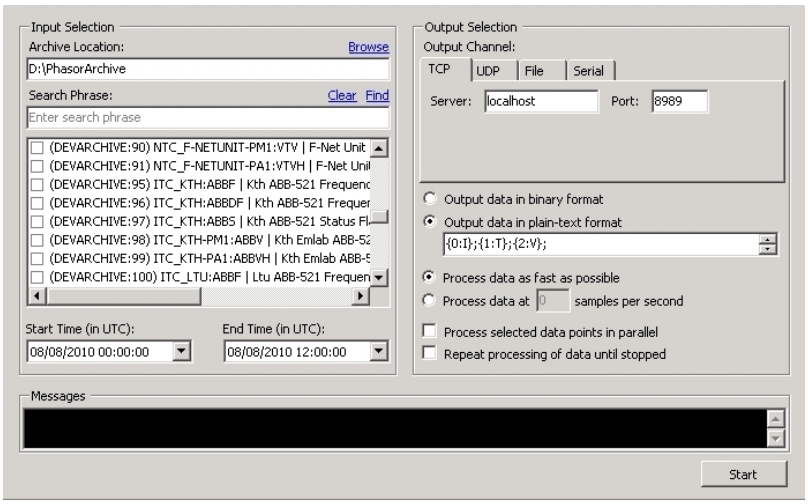

Figure 2.2: Historian Playback Utility.

2.3 MATLAB and MySQL

For efficient and fast handling of extracted data a relational database management system, MySQL, can be used to create a database from .csv files. One of the benefits of this approach is that the data that comes partially unsorted from openHistorian [1], now can be sorted in MySQL by the ascending order of the time-stamp. By importing the database to MATLAB we can use classes and data structures to organize the data and facilitate data processing and analysis.

A MySQL database connector [12] is used so that the MySQL database can be acessed from the MATLAB command prompt, imported to MATLAB and then saved in .mat format, Figure 2.3 below show the steps of this process.

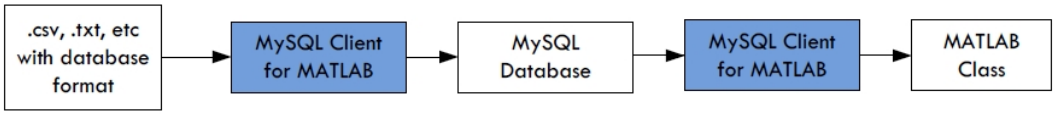

Figure 2.3: Conversion process from .csv to .mat using MATLAB and MySQL [13]

It is quite time consuming to manually perform all of the steps above every time files are to be converted. To simplify matters and save time, a small Graphical user interface (GUI) was constructed in MATLABs GUI Design Environment (GUIDE).

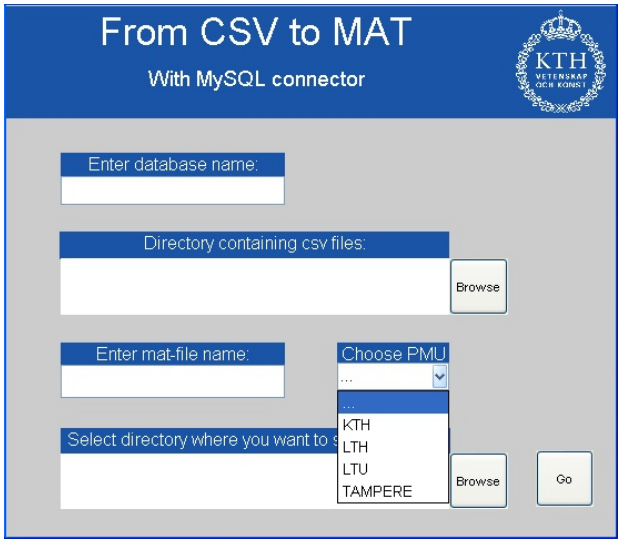

Figure 2.4: MATLAB built GUI used for conversion from .csv to .mat Manager installed at KTH showing frequencies derived in three different PMUs.

[1] In openPDC data is stored unsorted, before the time alignment and concentration process in a first arrived first stored basis

2.3.1 Data Conversion Process

It is useful to document the procedure used in this thesis to create MySQL database from .csv files and then save them to .MAT files. To this aim the GUI that handles the conversion process from .csv to .mat performs the following steps in a MATLAB script (which can also be carried out using the MATLAB command prompt):

- Open a connection to MySQL.
- Create and select the MySQL database to be used.
- Create a MySQL table with the columns: 'Point ID', 'Time Tag' and 'Value'.
- Search a folder for .csv files.
- Load the data from .csv files into the table.
- Import data to MATLAB from the tables and then sort the data by ascending order of the time-stamp.
- Save the sorted data to .mat files, frequency, voltage angle and voltage magnitude is saved in separate files.
- Delete the MySQL database.

The following need to be specified in the GUI:

- MySQL database name
- Name of .mat files
- Folder to search for .csv files
- Folder in which to save the .mat files
- Device from which to import data.

The .mat files will be saved as 'name'_ f, 'name'_ vang and 'name'_ vmag.

2.3.2 Installation Procedure of the MATLAB GUI

In order for the MATLAB GUI to work additional software needs to be installed, the GUI was developed in Microsoft Windows XP 32 bit[2] with MATLAB R2009B.

1 MySQL

Download and install MySQL server from

http://www.mysql.com/downloads/

2 C++ compiler

Make sure to have a C++ compiler installed (for example Microsoft Visual C++) and that it is selected in MATLAB, give the command mex -setup from the MATLAB command prompt to perform the configuration.

3 MySQL Database Connector

Download mysql.m, mysql.dll and libmysql.dll from

http://mmf.utoronto.ca/resrchres/mysql/

Put mysql.dll and mysql.m into MATLAB/toolbox/local/ or keep them in your working directory.

Put libmysql.dll into C:/WINDOWS/system32/.

5 Edit GUItest.m and createDatabase.m.

The MySQL password has to be given each time the connection is opened, edit the password in createDatabase.m at line 6.

Make sure the pointIDs for the devices are correct in GUItest.m line 231,233,235 and 237.

pmuData=['frequency' 'voltage angle' 'voltage phase angle'];

6 Run GUItest.m to start the GUI.

Instructions for GNU, Linux or Unix can be found at:
http://mmf.utoronto.ca/resrchres/mysql/

[2] The MySQL Database Connector is not compatible with 64 bit operating systems.

Chapter 3

Preprocessing

It is not uncommon for PMU data to have data quality issues. Before using phasor measurement data for mode estimation purposes, the data must be curated or preprocessed to remove flawed, redundant and irrelevant data. In addition, when deterministic data errors are known, it is possible to add estimates of missing samples or to correct these errors.

3.1 Timestamp Errors

There are a few time stamp related problems that have to be taken care of. First, PMUs sometimes fail to update information from each sample resulting in sequences of samples with identical values. Second the PMUs may have firmware issues[1] which incorrectly places all the timestamps in the first quarter of each second, see Fig.3.1

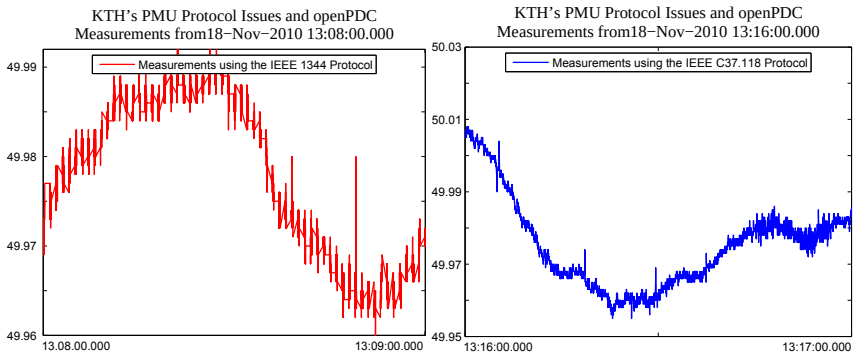

(a) (b)

Figure 3.1: Frequency provided under (a) IEEE 1344 (b) IEEE C37.118 protocol transmission

[1] Results from a protocol change test - At KTH a PMU has been changed from the IEEE 1344 to the IEEE C37.118 protocol. The plots in Fig.3.1 show that the PMU might have issues with transmitting data correctly in the IEEE 1344 protocol. However, the source of this error has not been fully identified and it might be related to the IEEE 1344 protocol parser in openPDC (although no similar issues have been reported by the openPDC community [9]).

The problem of samples with identical values is solved by simply removing duplicates, for the second problem an algorithm is designed to perform the following steps:

1 The time stamps are of the form 'dd-mmm-yyyy HH:MM:SS.FFF' and it is the FFF stamp that is incorrect. So the first issue that must be addressed is to examine the possible values of the FFF stamps, since there is a sampling frequency of 50 Hz this means that there should be 50 unique stamps.

2 Index all the FFF stamps so that the first (in chronological order) will have index 1 and the last will have index 50.

3 Replace all the timestamps according to the following formula[2]

$$newFFF = 20(i - 1) \tag{3.1}$$

here i is the index of the stamp and 20 is the sampling period (20 ms). The index i=1,2,.., 50 will result in FFF stamps 000, 020,..,980 (note that this requires zeros to be added in the leading edge to obtain the correct format).

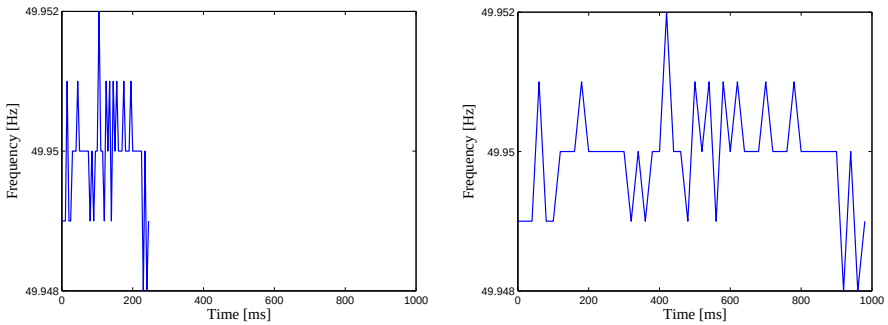

(a) (b)

Figure 3.2: Frequency from Tampere's PMU showing: (a) Samples incorrectly placed (b) Samples redistributed with the above algorithm

[2] There are a total of 50 unique FFF stamps in the original data and each one of these will correspond to one of the new stamps. So if one sample is missing in the original data the corresponding sample in the curated data will also be missing.

3.2 Interpolation

The data extracted from the Historian Playback Utility has missing samples. This might be due to PMU sensing, processing or communication failure [14], however, another reason for missing samples is that the extraction process from the database suffers from imperfections. From our experience working with the HPU data extraction can be inconsistent. Extraction of the same data set can result in different amounts of extracted data. From Table 3.1 it is possible to get a general notion as to the amount of samples that are being lost in the conversion process with the HPU.

Extraction Nr.	Extracted Lines	Missing Samples
1	179931	69
2	179948	52
3	179946	44
4	179973	27
5	179983	17
6	179984	16
7	179991	9
8	179949	51
9	179955	45
10	179937	63

Table 3.1: Amount of extracted lines for a 1 hour period, same period extracted ten times.

Regardless of the source of this error, missing samples can be estimated from other samples using interpolation. In this way the new data vectors will be complete and have a uniform distance between each sample. Linear interpolation will give a good sample estimate, but this is of course limited to small sections of missing data. In addition, under most operating conditions data is obtained at a high sampling frequency, and so the sampled data will change very little between each phasor measurement [3].

[3] Note that this may not apply for data from large disturbances.

Because we are interested in the frequency region up to 2 Hz the fastest dynamics we need to take into consideration is a 2 Hz oscillation, in Fig.3.3 such a oscillation is illustrated.

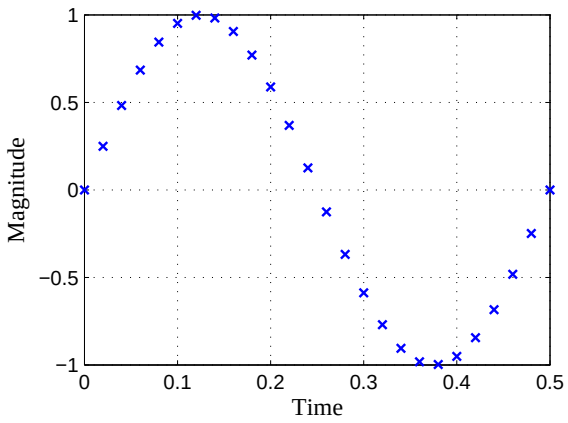

Figure 3.3: 2 Hz oscillation, 50 Hz sampling rate.

For the used sampling rate, 50 Hz, there are 25 samples distributed over the period of the oscillation, as long as there is not more than 2 or 3 samples missing linear interpolation will give good estimates. But in cases when there are larger blocks of missing data, interpolation will not yield good estimates and should therefore be avoided. In this thesis, a threshold has been set, sections of missing samples that are longer than 3 samples have not been interpolated[4], and are threated as missing data.

[4] Loss of individual samples represent the majority of the missing samples, the data used in this thesis have no sections of missing samples longer than 3 samples

The algorithm used in this thesis to perform interpolation has been designed using the following steps:

1 Create a complete time vector.

2 Create two complete value vectors, one using linear and one using nearest neighbor interpolation.

The nearest neighbor interpolation, illustrated in Fig.3.4a, selects the value of the closest sample. So existing samples will stay unchanged[5].

With linear interpolation, illustrated in Fig.3.4b, a sampled value at time t is calculated with the formula

$$f = f_0 + \frac{(t - t_0)f_1 - (t - t_0)f_0}{t_1 - t_0} \tag{3.2}$$

(t_0, f_0) and (t_1, f_1) is the closest preceding and following sample.

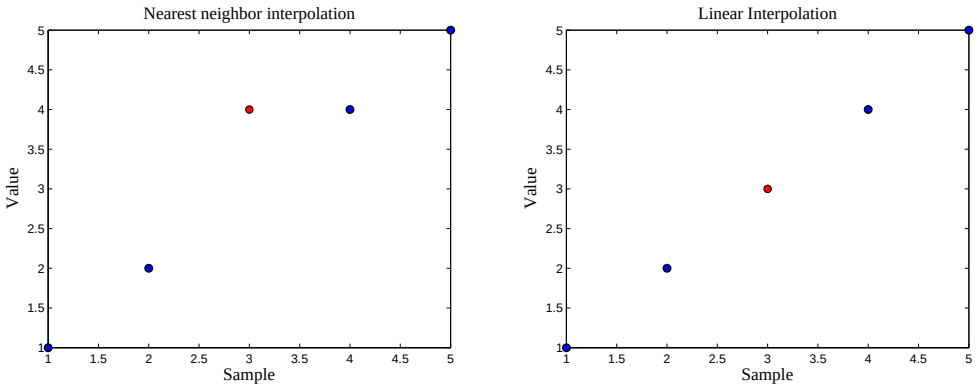

(a) (b)

Figure 3.4: Sample 3 (shown in red) is missing and has been interpolated with (a) nearest neighbor interpolation (b) linear interpolation

3 Find all the missing samples and put their index in a vector.

4 Build a new complete vector of values. The nearest neighbor interpolated vector will contain all the existing samples, use this vector but replace all the nearest neighbor estimates of missing samples with the linearly interpolated values.

5 Remove all sections of missing samples that are longer than 1 second.

[5] If the distance to two samples is equal, the value of the subsequent sample is selected

3.3 Detrending

Because of system frequency control there will be slow gradual changes in the measured signals, such characteristic is a signature of governing-control actions, and hence the mean value of the frequency will change over time. However, methods used for spectral analysis require data from a stochastic process to be able to work properly. To obtain this random signal (ambient data) which only depends on random load-variations in the system, the effects of governing-control need to be removed. Consequently, linear trends are removed and the mean subtracted, so that the signals fluctuates with reference to the same value over the whole interval.

Detrending can be done by using MATLAB's detrend function and a FIR high-pass filter. The filter cutoff frequency is selected so that there is little attenuation in the frequency region of interest, which is the region were electromechanical modes are located 0.1-2 Hz. A filter of order 1500, with 0.07 Hz cutoff frequency provides good attenuation properties close to the cutoff frequency of 0.1 Hz. Fig.3.5 shows the frequency response of the high-pass filter while Fig.3.6 shows the signal before and after detrending[6].

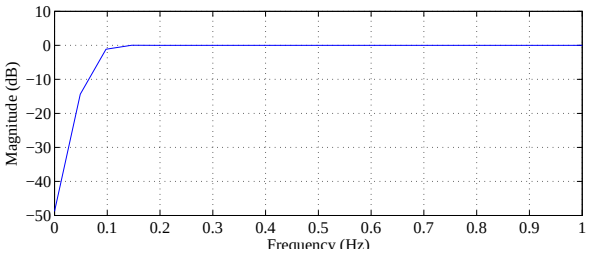

Figure 3.5: High-pass filter of order 1500 and 0.07Hz cutoff frequency.

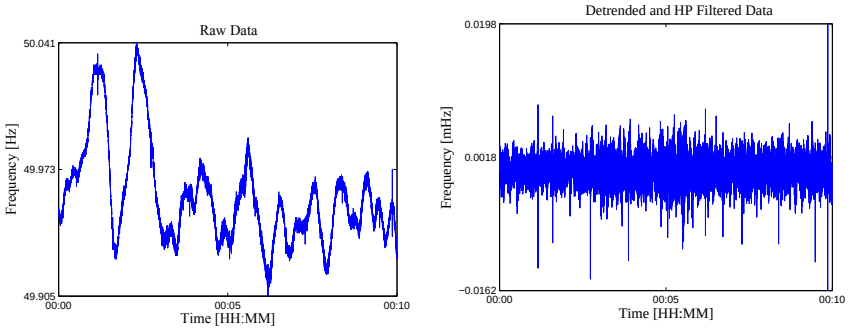

(a) (b)

Figure 3.6: Ten minutes of (a) raw data (b) detrended from Tampere's PMU.

[6] Observe that the filter design used for detrending depends on the frequency dynamics of each network, in the Nordic power system there is a more loose frequency regulation then that in the Eastern interconnection of the U.S. Therefore the signatures of each power system as provided by PMUs must be first analyzed to determine good filter design specifications.

3.4 Outlier Removal

An outlier is a sampled value that is subject to measurement error and therefore deviates significantly from the majority of the other samples. These samples will need to be removed so that they do not have a negative effect on the methods used for ambient data analysis.

Samples that deviate more than 5 standard deviations from the mean of the signal are here defined as an outlier and thus removed. Fig.3.7 shows how outliers are removed from the signal.

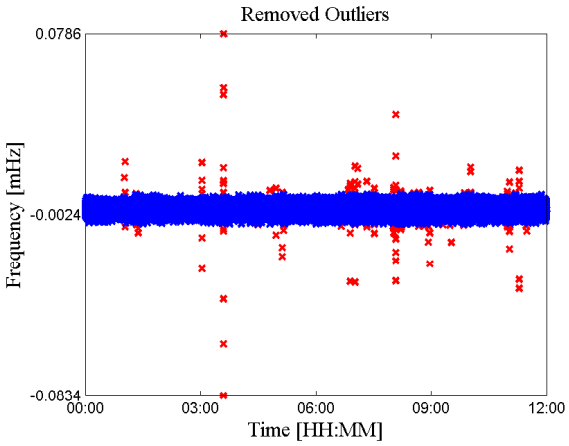

Figure 3.7: Twelve hours of data from Tampere's PMU showing removed outliers (red dots)

From the Fig.3.7 it can be seen that most of the outliers are concentrated to short periods of time, it is likely that many of theses outliers are minor transients and therefore not necessarily caused by measurement errors. These transients are not significant, and because the aim of preprocessing is to obtain ambient data, this approach for removal of outliers in the data will provide adequate data for ambient analysis.

3.5 Downsampling

Sampling rates that are significantly faster than the power systems electromechanical dynamics will result in redundant data with relatively low information content in each new sample. On the other hand, sampling rates that are too slow will create difficulties when it comes to estimating electromechanical mode properties. Furthermore, when using parametric methods (such as Yule-Walker parametric estimation), the autocovariance matrix used by these methods will become ill-conditioned for high sampling frequencies. Consider for example the conditioning of the Yule-Walker autocovariance matrix show in Fig.3.8.

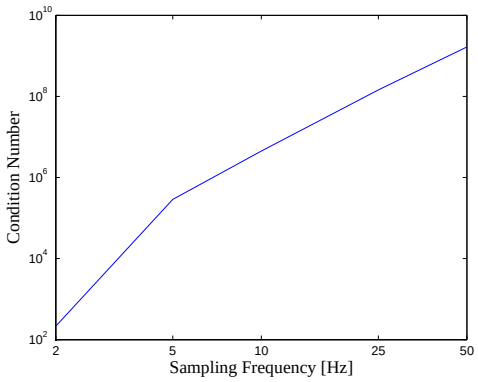

Figure 3.8: Condition number of the Yule-Walker autocovariance matrix for different sampling frequencies.

As can be seen from Fig.3.8 the sampling frequency should, for sake of conditioning, be kept as low as possible. The problem is then to determine how much the signal can be downsampled without loosing valuable information. This can be done by comparing spectral estimates computed using different sampling frequencies.

Because different number of samples will be used for each of the estimates, we can expect the estimates to vary slightly. Nevertheless, the difference between the estimates in Fig.3.9 is very small, and therefore we can conclude that for the 50 Hz, 25 Hz and 10 Hz sampled data, the estimates are using a large amount of redundant data. However it is not possible to reduce the sampling frequency much further below 5 Hz because when a signal is downsampled below this threshold, information about the frequencies higher than half of the sampling frequency is lost [15]. Thus, it is not possible to construct a spectral estimate for the desired frequency range (0.1-2 Hz) if the sampling frequency is selected lower than 4 Hz.

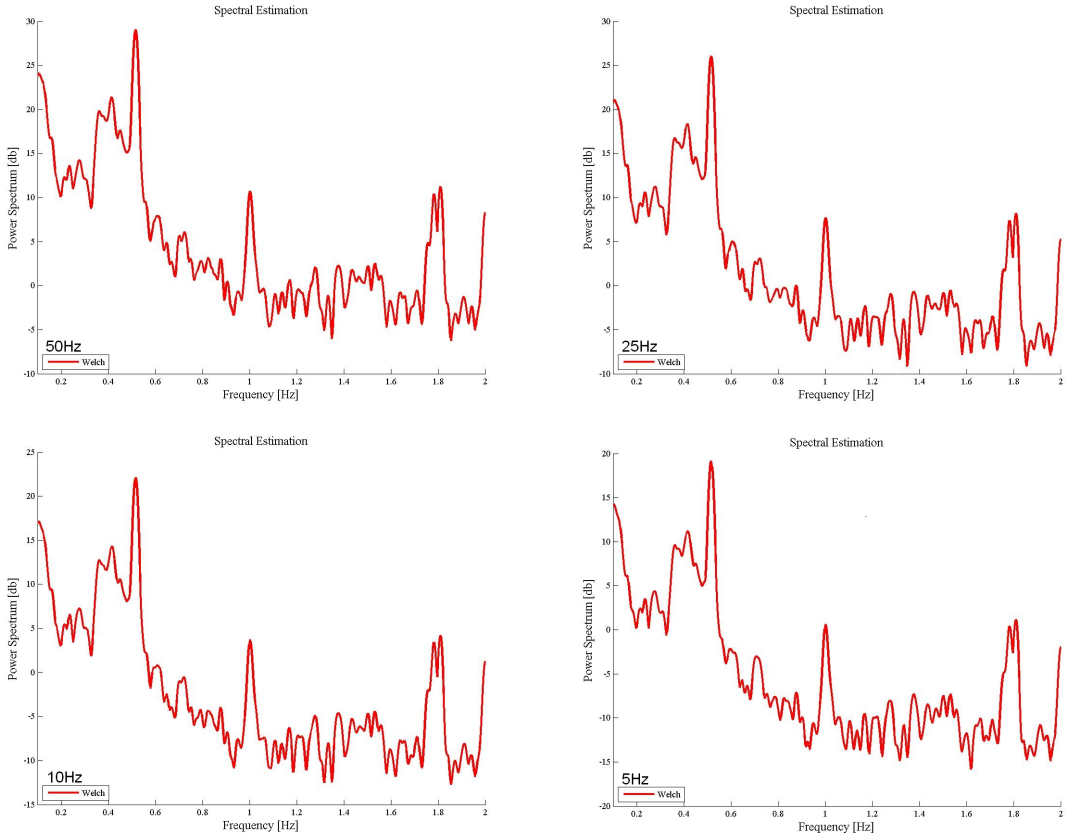

Figure 3.9: Welch Spectral estimates computed with 5Hz, 10Hz, 25Hz and 50Hz sampling frequency and using 10 min of data from Tampere's PMU.

Aliasing occurs when frequencies higher than one half of the sampling rate are present, this results in that the high frequency components look like low frequency components. To avoid errors due to aliasing the data must be passed through a low-pass filter before it is downsampled. The filter should remove all frequencies above the Nyquist frequency, to this end, a FIR low-pass filter of order 1500 and with cutoff frequency 2.4 Hz is used. The frequency domain characteristic of this filter is shown in Fig.3.10.

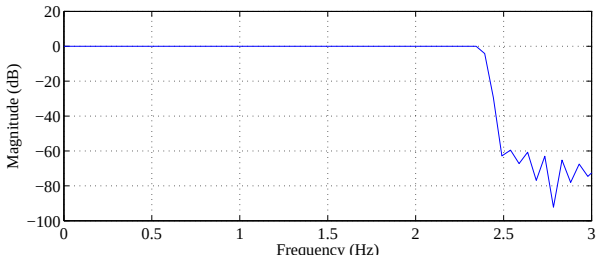

Figure 3.10: Low-pass filter of order 1500 and 2.4Hz cutoff frequency.

Chapter 4

Mode Frequency Estimation

4.1 Introduction

Spectral analysis has a wide range of uses in many diverse fields, and can be used to obtain valuable information about a multitude of systems. By estimating the power spectral density from a stationary process, periodicities which are related to the dynamical behavior of a system may be detected. Consequently we can use a random signal (ambient data) which only depends on random load-variations in the system to gain some insight into the dynamics of the Nordic power system.

The relationship between the excitation input $u(t)$ and the output $y(t)$ of a system can be expressed in the frequency domain by

$$S_{yy}(\omega) = S_{uu}(\omega)|H(\omega)|^2 \tag{4.1}$$

were $S_{uu}(\omega)$ and $S_{yy}(\omega)$ are the input and output power spectral density (PSD) matrices and $H(\omega)$ is the frequency response function (FRF), which can be described by

$$H(\omega) = \sum_{i=1}^{N} \left(\frac{A_i}{j\omega - \lambda_i} + \frac{A_i^*}{j\omega - \lambda_i^*} \right) \tag{4.2}$$

where i is the mode index, N number of modes, A_i residue, λ_i pole and ω mode frequency [16].

Pole locations, and hence the modal frequencies, will show up as peaks in the output PSD function. So if the PSD can be estimated from an available time series, this will in turn give a estimate of mode frequencies. There exist many methods for PSD estimation, those utilized here and their methodology are described in [17].

4.2 Spectral Estimators

4.2.1 Parametric Spectral Estimation

Assume that the PSD of a process can be completely described by k parameters $a_1, a_2, .., a_k$

$$S(f) = S(f, a_1, a_2, .., a_k) \tag{4.3}$$

and that these parameters can be estimated from observations $X_1, X_2, \ldots, X_N$ of the system.

The PSD can then be estimated with

$$\hat{S}(f) = S(f, \hat{a}_1, \hat{a}_2, .., \hat{a}_k) \tag{4.4}$$

In the following section the Yule-Walker equations are used to estimate the parameters $\hat{a}_1, \hat{a}_2, \ldots, \hat{a}_k$.

4.2.2 Yule-Walker Spectral Estimator

The Yule-Walker Spectral Estimator utilizes the autoregressive model of order p

$$Y_t = \phi_{1,p} Y_{t-1} + \phi_{2,p} Y_{t-2} + ... + \phi_{p,p} Y_{t-p} + \epsilon_t \tag{4.5}$$

where Y_t is a zero mean stationary process and $\phi_{1,p}, \phi_{2,p}, \ldots, \phi_{p,p}$ are the model coefficients. ϵ_t is a white noise process with zero mean and variance σ_p^2.

The PSD is then given by

$$S(f) = \frac{\sigma_p^2 \Delta t}{|1 - \sum_{j=1}^{p} \phi_{j,p} e^{-i2\pi f_j \Delta t}|} \tag{4.6}$$

To obtain the model coefficients (4.5) is multiplied with Y_{t-k}, and then the expectation is obtained in order to determine the autocovariance sequence s_k.

$$s_k = E[Y_t Y_{t-k}] = E\left[\sum_{j=1}^{p} \phi_{j,p} Y_{t-j} Y_{t-k} + \epsilon_t Y_{t-k}\right] = \sum_{j=1}^{p} \phi_{j,p} s_{k-j} \tag{4.7}$$

here we use the fact that $E[\epsilon Y_{t-k}] = 0$ for $k > 0$.

And so the Yule-Walker equations can be formulated

$s_1 = \phi_{1,p}s_0 + \phi_{2,p}s_1 + ... + \phi_{p,p}s_{p-1}$
$s_2 = \phi_{1,p}s_1 + \phi_{2,p}s_2 + ... + \phi_{p,p}s_{p-2}$
.
.
.
$s_p = \phi_{1,p}s_{p-1} + \phi_{2,p}s_{p-2} + ... + \phi_{p,p}s_0$

or in more compact form

$$\gamma_p = \Gamma_p \phi_p \tag{4.8}$$

Multiplying the inverse of Γ_p with γ_p yield the coefficients

$$\phi_p = \Gamma_p^{-1} \gamma_p \tag{4.9}$$

By using an available time series $X_1, X_2, .., X_N$ we can produce estimates of s_k and then use them to estimate the model coefficients, as follows:

$$\hat{s}_k = \frac{1}{N} \sum_{t=1}^{N-|k|} X_t X_{t+|k|} \tag{4.10}$$

$$\hat{\phi}_p = \hat{\Gamma}_p^{-1} \hat{\gamma}_p \tag{4.11}$$

σ_p still has to be estimated and this can be done by once again using the fact that $E[\epsilon Y_{t-k}] = 0$ for $k > 0$. To this end

$$s_0 = \sum_{j=1}^{p} \phi_{j,p} s_j + E[\epsilon_t Y_t] \tag{4.12}$$

$$E[\epsilon_t Y_t] = E\{\epsilon_t (\sum_{j=1}^{p} \phi_{j,p} Y_{t-j} + \epsilon_t)\} = \sigma_p^2 \tag{4.13}$$

and hence σ_p^2 can be estimated by

$$\hat{\sigma}_p^2 = \hat{s}_0 - \sum_{j=1}^{p} \hat{\phi}_{j,p} \hat{s}_j \tag{4.14}$$

The complete PSD estimator can now be constructed

$$\hat{S}(f) = \frac{\hat{\sigma}_p^2 \Delta t}{|1 - \sum_{j=1}^{p} \hat{\phi}_{j,p} e^{-i2\pi f j \Delta t}|} \tag{4.15}$$

4.2.3 Nonparametric Spectral Estimation

The key concept in nonparametric spectral estimation is to use the following relation between the autocovariance sequence and the PSD

$$S(f) = \Delta t \sum_{\tau=-\infty}^{\infty} s_\tau e^{-i2\pi f \tau \Delta t} \tag{4.16}$$

and to consider a zero mean stationary time series of N observations to estimate the autocovariance sequence for $\tau = 0, \pm 1, ..., \pm(N-1)$.

$$\hat{s}_\tau = \frac{1}{N} \sum_{t=1}^{N-|\tau|} X_t X_{t+|\tau|} \tag{4.17}$$

this estimate can be included into (4.16) to obtain the estimator:

$$\hat{S}(f) = \frac{\Delta t}{N} \left| \sum_{t=1}^{N} X_t e^{-i2\ pif\tau\Delta t} \right|^2 \tag{4.18}$$

This function is known as the periodogram. There are some major drawbacks with this type of estimators, the most important being high variance as well as severe bias.

Most of the periodograms bias is due to spectral leakage which can be mathematically explained as follows. The expected value of (4.18) can be written as

$$E\{\hat{S}(f)\} = \int_{-f_N}^{f_N} F(f - f') S(f') df' \tag{4.19}$$

where

$$F(f) = \frac{\Delta t\ sin^2(N\pi f \Delta t)}{N sin^2(\pi f \Delta t)} \tag{4.20}$$

where F(f) is called Fejèrs kernel. A peak at a particular frequency in the frequency domain will result in smaller peaks, due to the side lobes of Fejérs kernel, in the nearby frequency range (i.e. spectral leakage).

There are a few ways, as we shall see, to modify the periodogram to get a estimator with better variance and bias properties.

4.2.4 Welch's Spectral Estimator

Welch's estimator is a modified version of the periodogram described in the previous section. The following steps are performed to form this estimator:

1. Split the original N observations into N_B overlapping blocks with N_S samples each.

   To reduce the variance of the periodogram, several periodograms are computed and then averaged together. The reduction in variance will be proportional to the number of blocks (i.e. the number of periodograms computed). Nevertheless this reduction comes at the expense of lowered spectral resolution.

   By allowing the blocks to overlap, additional blocks are obtained and hence further reduction in variance is achieved. The overlap will also recover some information that will be lost later due to tapering the data and hence down weighting some samples in each block. An overlap of 50 percent will recover much of this information. But the overlap should not be increased above this level since that might actually result in a loss of some of the recovered information.

2. Apply a data taper, h_t, on each block.

   To reduce the bias due to spectral leakage it is recommended that every block is windowed with a Hanning data taper [1], as the one shown in Fig.4.1. This will reduce the sidelobes of Fejérs kernel and hence the bias caused by spectral leakage.

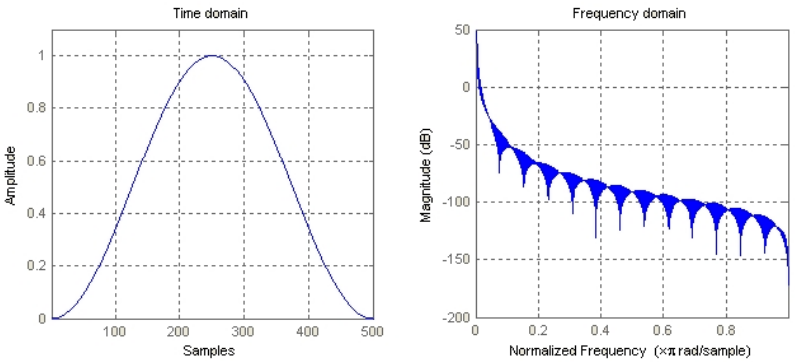

Figure 4.1: Hanning data taper and associated spectral window

[1] Other windows such as the Hamming window can also be used

As can be seen from the Fig. 4.1, the Hanning data taper effectively attenuates the sidelobes.

3. Obtain a periodogram for each block.
4. Average the individual periodograms together to form an overall spectral estimate.

The resulting spectral estimator will be given by

$$\hat{S}(f) = \frac{\Delta t}{N_B} \left| \sum_{j=0}^{N_B-1} \sum_{t=1}^{N_s} h_t X_{t+jn} e^{-i2\pi f_t \Delta t} \right|^2 \tag{4.21}$$

were n is a integer specifying the amount of overlap between each block.

4.2.5 Multitaper Spectral Estimator

Suppose we have the time series $X_1, X_2, ..., X_N$ with zero mean and variance σ^2. For a sequence of K data tapers, $h_{t,k}$, we can then compute K individual eigenspectrums as follows:

$$\hat{S}_k(f) = \Delta t \left| \sum_{t=1}^{N} h_{t,k} X_t e^{-i2\pi f t \Delta t} \right|^2 \tag{4.22}$$

The tapering will reduce bias in the estimator, and if the average of all these eigenspectrums are obtained, the variance of the resulting estimator will also be reduced. The estimator will therefore be given by

$$\hat{S}(f) = \frac{1}{K} \sum_{k=0}^{K-1} \Delta t \left| \sum_{t=1}^{N} h_{t,k} X_t e^{-i2\pi f_t \Delta t} \right|^2 \tag{4.23}$$

To get a good reduction in both bias and variance it is of great importance to select a sequence of data tapers that not only have good leakage properties, but also have relatively uncorrelated eigenspectrums. If the spectrums are to highly correlated it wont be possible get the desired reduction in variance. When data tapers are orthogonal, it is possible to obtain a sufficient degree of uncorrelation in a sequence of tapers, therefore:

$$\sum_{N}^{t=1} h_{t,j} h_{t,k} = 0 \quad j \neq k \tag{4.24}$$

The discrete prolate spheroidal sequences (dpss) fulfill these requirements and are therefore frequently used with multitaper spectral estimators.

4.3 Simulations

To verify that the mode estimation algorithms in this Chapter perform correctly, simulations are carried out. A model of the Southern/Southeastern Brazilian power system [19] of similar structure to the model described in Section 1.2 is used for purpose. The model consists of seven buses and five synchronous generators that are described by a fifth-order model, the system model is illustrated in Fig 4.2.

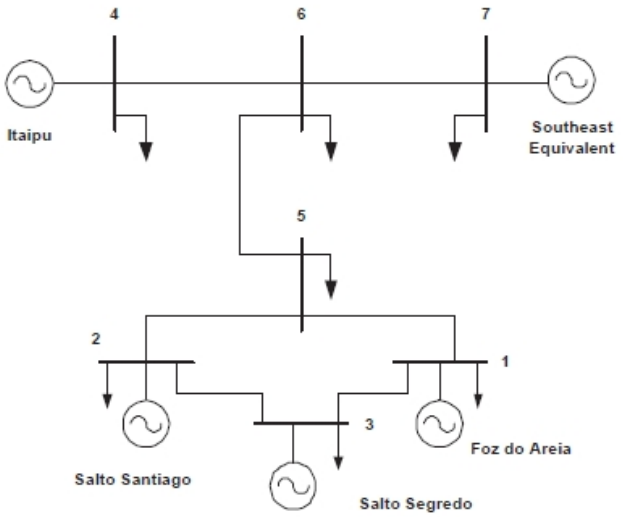

Figure 4.2: Model of the Southern/Southeastern Brazilian power of system.

The system has been stabilized using Power System Stabilizers so most of the modes are well damped, but there are three modes with relatively low damping. The mode frequency and damping of these modes are given in Table 4.1.

Mode	Frequency (Hz)	Damping (%)
1	0.8328	6.93
2	1.8060	14.54
3	1.9433	10.63

Table 4.1: Mode frequency and damping of the modes with low damping.

The 0.83 Hz mode is an inter-area mode, the 1.80 Hz and 1.94 Hz modes are local modes. We focus our analysis in this Section on the 0.83 Hz mode.

By using white noise as input to all load buses, and the active power flow in the tie-line between the systems as the system output, ambient data can be obtained, see Fig.4.3. In the simulations performed the active power flow in the transmission line connecting Bus 6 to 7 was used as output with the aim of capturing the inter-area mode. The 1.80 Hz local mode, the 1.94 Hz local mode are due to oscillations in other parts of the system and will not be of concern here. Also observe that because of the signal selected for ambient data analysis, these local modes will not necessarily be observable. This fact is supported by theory in [20].

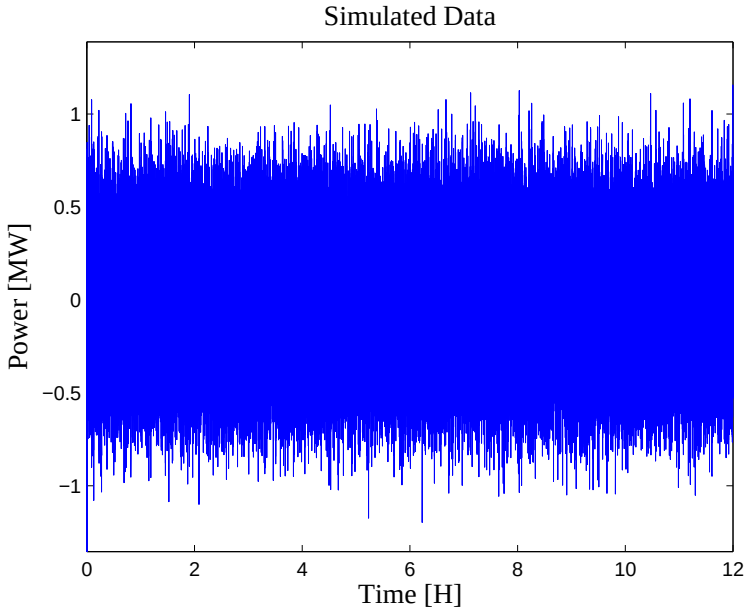

Figure 4.3: 12 h of simulated data from the system in Fig.4.2.

From Fig.4.4 it can be seen that the algorithms is able to capture both the inter-area mode and the local mode, the inter-area mode is much easier to determine because it is more narrow which comes from its low damping ratio.

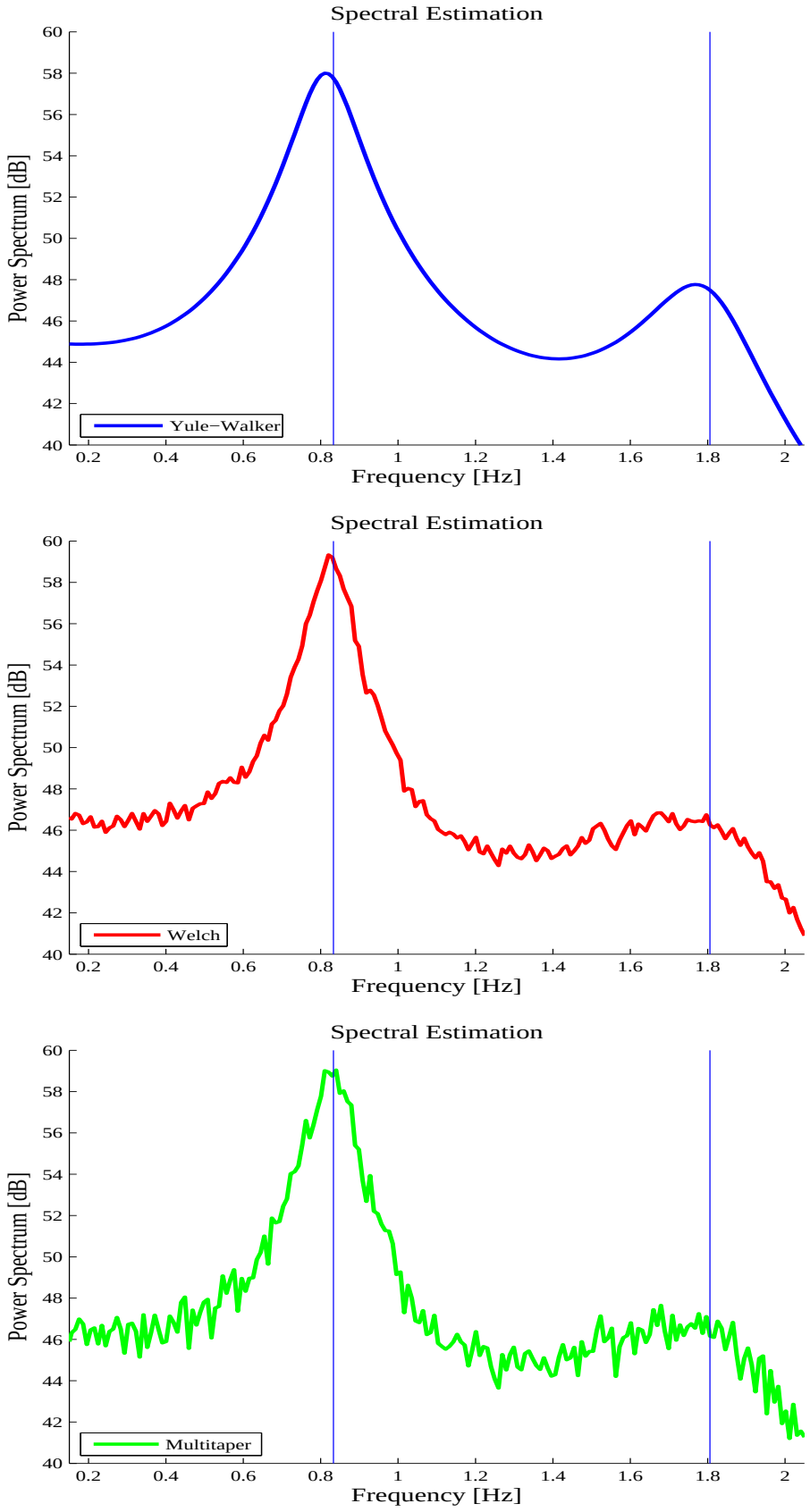

Figure 4.4: Yule-Walker, Welch and Multitaper spectral estimates using 12 h of simulated data.

4.4 Forced Oscillations

There are forced oscillations (or undamped sinusoids) of unknown origin in the data sets. These oscillations will show up as narrow band oscillations in the PSDs and if superimposed over a real system mode they will cause problems to obtain good damping estimates. FFTs (Fast Fourier Transforms) can be used to examine the data and identify forced oscillations.

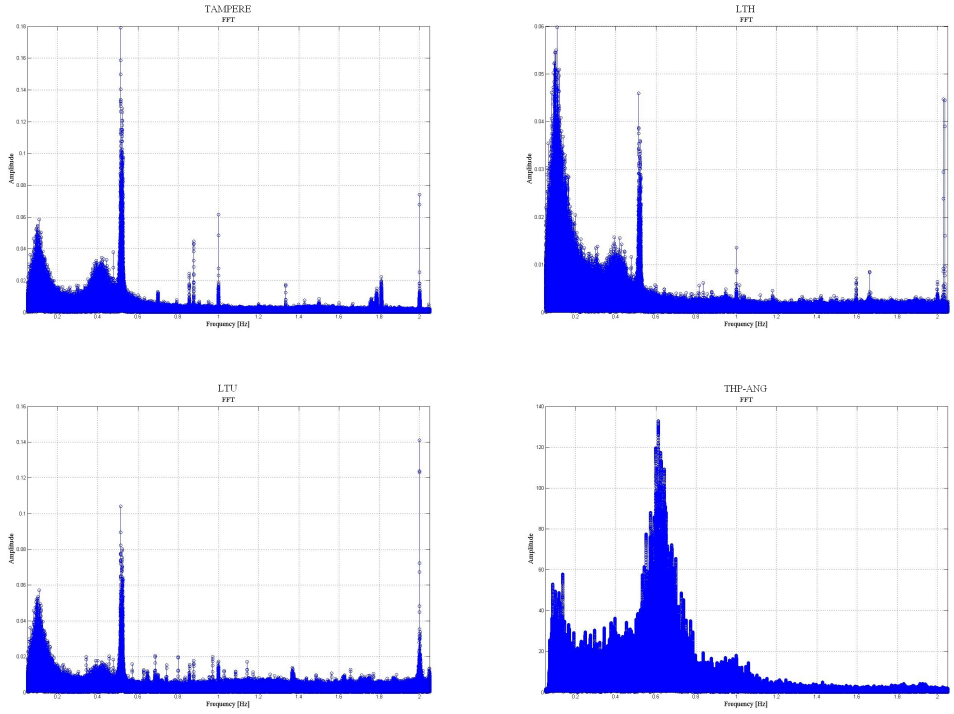

Figure 4.5: FFTs for Tampere, LTH, LTU using 12 h of data and THP-ANG using 3 h.

There appears to be forced oscillations in all three data sets (LTH, LTU, Tampere) at exactly 1Hz and 2Hz. To rule out that these oscillations are somehow caused by the algorithms used a fourth FFT is computed using data from the Mexican power system. As can be seen from Fig.4.5 there are no such oscillations present in this data.

Forced oscillations in Nordic PMU data have been previously evidenced in [18]. These results show that the forced oscillations are of natural appearance in the Nordic grid as the measurements were taken from different devices and locations than those from [18].

4.4.1 Forced Oscillation Analysis using Nonparametric Spectrograms

For a sufficient amount of data, nonparametric spectral estimators (such as Welch) can be expected to produce high resolution PSDs with low variance and low bias. Consequently the Welch Spectral Estimator will, for a sufficient amount of samples, give a good overview of the location of the electromechanical modes in the system, and to classify between true system modes and forced oscillations.

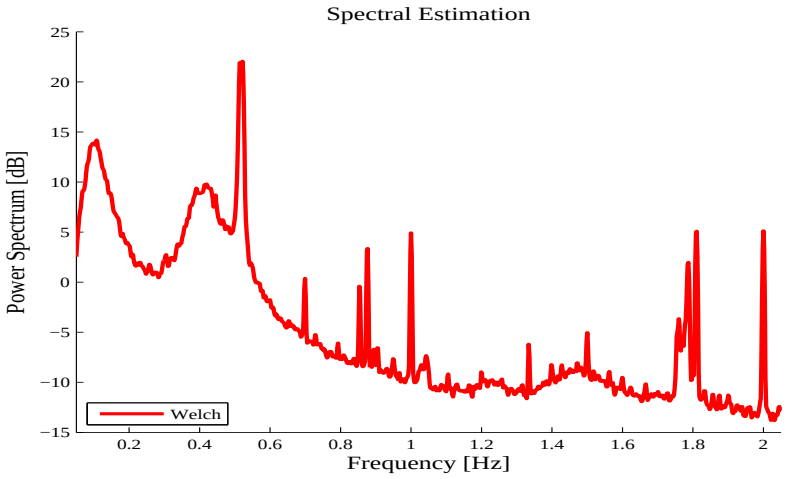

Figure 4.6: Welch Spectral Estimate, 12h of data from Tampere's PMU and 1440 samples block size.

This estimate can also be of great help when determining appropriate parameters i.e block size, number of tapers and model order for estimators using significantly less data.

A spectrogram shows how the spectral density of a signal varies with time, it can therefore be used to study variations and small fluctuations of modes in a power system. To get a spectrogram with reasonable resolution the individual PSDs must be computed with relatively few samples, in this case we use 10 minutes of data with a 90 percent data overlap[2] between two successive PSDs.

To determine parameters for the different estimators several spectrograms can be computed using different parameter values and then be compared to the 12 hours PSD in Fig.4.6. The spectrogram that is able to most clearly capture the modes, and will thus indicate the adequate number of parameters to be used.

[2] Note that this overlap is on the preprocessed data, and not the overlap used by the spectral estimators. Hence, there are no issues with loss of information as discussed in section 4.2.4. The important difference to note here is that overlaps are used to create a large number of PSDs which can give a high resolution spectrogram.

Welch Spectral Estimator - Block Size

From Section 4.2.4 we know that a decreased block size leads to a decrease in variance and a lowered spectral resolution. By starting with a large block size and slowly decrease it until the peaks can be distinguished from the variance it is possible to obtain a PSD with acceptable variance while lowering the spectral resolution as little as possible.

For a block size of 1000 samples the peaks of large amplitude are visible in the spectrogram, but smaller peaks are buried in the variance. By decreasing the block size the $\sim$0.7Hz peak soon becomes visible but for the smallest peaks ($\sim$1.4Hz and $\sim$1.5Hz) it is necessary to decrease to 500 samples to obtain decent visibility.

A 12h Welch Spectrogram using 500 samples block size is shown in Fig.4.7 and a 10 min PSD with the same block size is shows in Fig.4.8. By studying the frequency region 1.2-1.8Hz in the PSD it can be seen why the peaks in this region are hard to make out in the spectrograms, the dynamic range in this region is simply too low compared to the variance of the estimates.

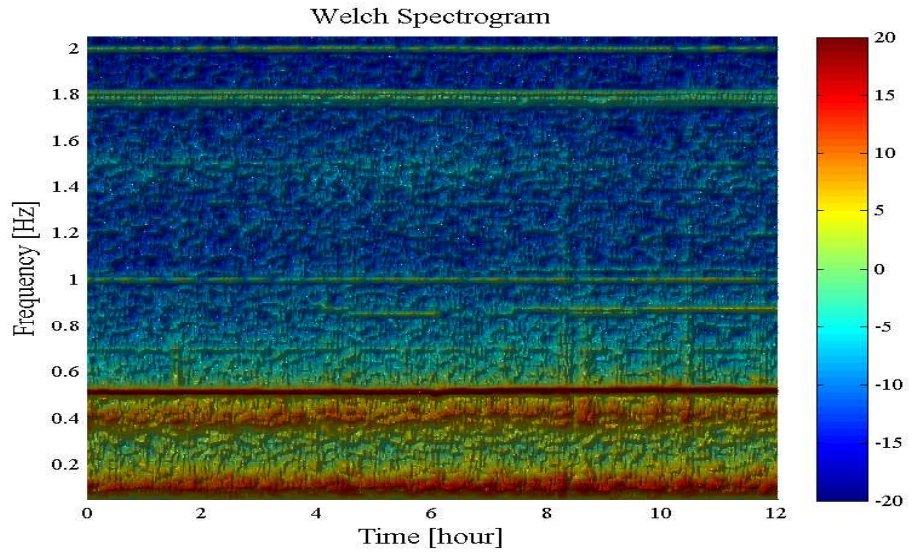

Figure 4.7: Welch Spectrogram, 12h of data from Tampere's PMU, 10min PSDs and 500 samples block size.

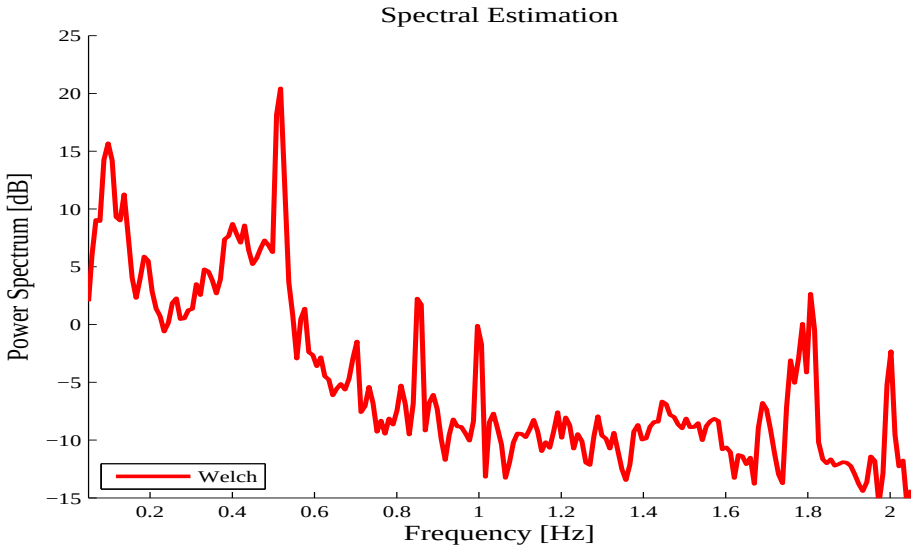

Figure 4.8: Welch Spectral Estimate, 10min of data from Tampere's PMU and 500 samples block size.

Multitaper - Number of Tapers

To determine an appropriate number of tapers we can use an approach similar to that used for the Welch spectrogram. Since the variance decreases as the number of tapers increases we can begin with a small number of tapers and increase until the smaller peaks can be discerned from the variance.

For 3 tapers most of the peaks in Fig.4.6 are visible, but the smaller peaks are not because of variance. With 5 tapers the $\sim$0.7Hz peak becomes visible, but for the $\sim$1.4Hz and $\sim$1.5Hz peaks we need 8 tapers for sufficient variance reduction.

A 12h Multitaper Spectrogram using 8 tapers is shown in Fig.4.9 and a 10 min PSD with the same number of tapers is shows in Fig.4.10. Just as for the Welch Spectrogram the peaks outside the frequency region 1.2-1.8Hz can easily be made visible in the spectrogram, but the peaks inside this region are hard to make out due to the low dynamic range.

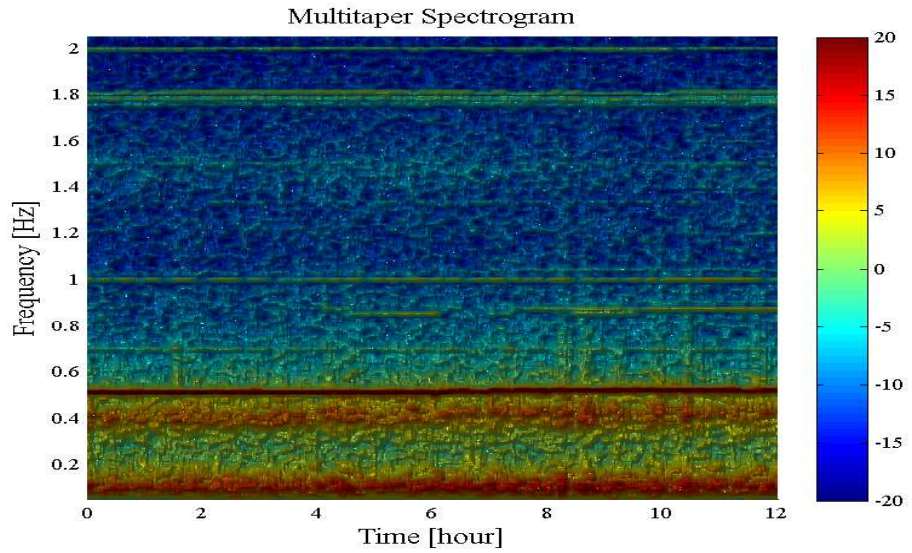

Figure 4.9: Multitaper Spectrogram, 12h of data from Tampere's PMU, 10min PSDs and 8 tapers.

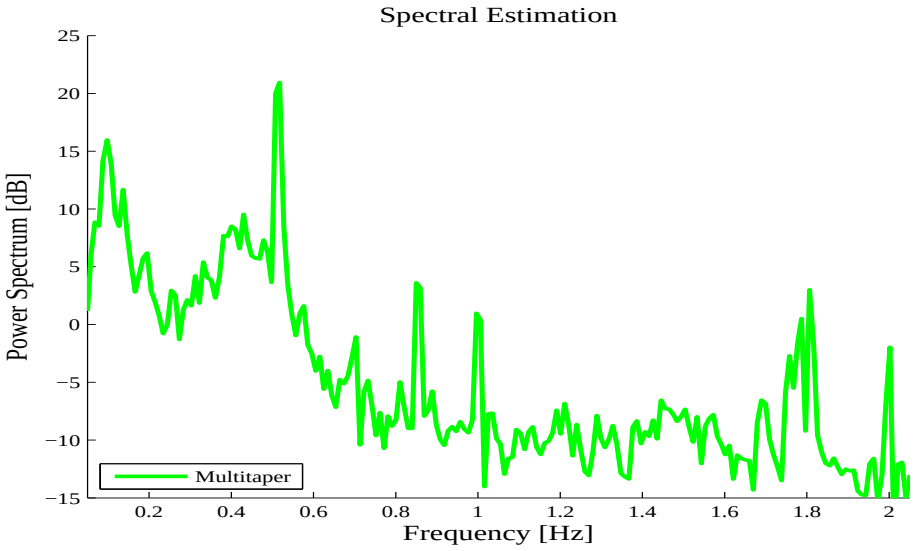

Figure 4.10: Multitaper Spectral Estimate, 10min of data from Tampere's PMU and 8 tapers.

Yule-Walker - Model Order

If the Yule-Walker model order is selected too high the spectrogram will be exhibiting artificial peaks, on the other hand an insufficient model order result in a spectrogram where some of the true peaks of the modal frequencies have not been captured.

By studying the visibility of the $\sim$0.7Hz and $\sim$0.8Hz peaks it can be determined that a model order 36-39 is appropriate. Further investigation of the peaks in the 1.2-1.6Hz region narrows this interval to a model order 38-39.

A 12h Yule-Walker Spectrogram using a model order 38 is shown in Fig.4.11 and a 10 min PSD with the same model order is shows in Fig.4.12. All the peaks that can be seen in the PSD can also, unlike the nonparametric estimators, be clearly seen in the spectrogram.

A systematic methodology to determine the model order of the Yule-Walker estimator using partial autocorrelation coefficients is discussed in section 5.2.

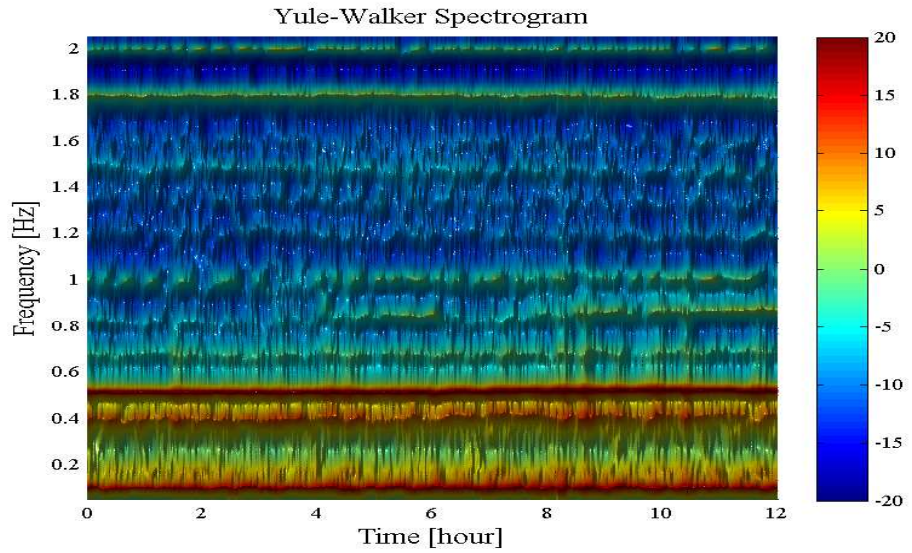

Figure 4.11: Yule-Walker Spectrogram, 12h of data from Tampere's PMU, 10min PSDs and model order 38.

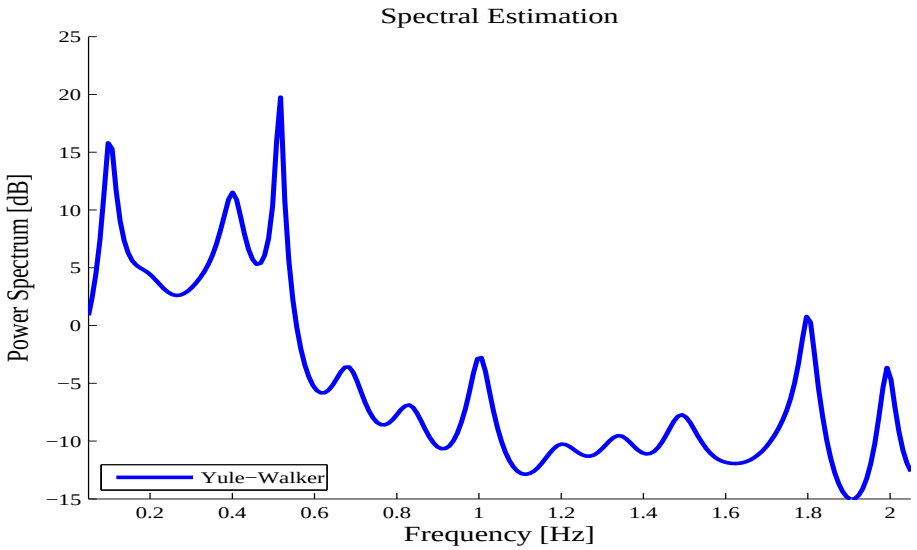

Figure 4.12: Yule-Walker Spectral Estimate, 10min of data from Tampere's PMU and model order 38.

4.5 Comparison of Spectral Estimators

Three different spectral estimators, Welch, Multitaper and Yule-Walker, have been used to compute spectrograms and PSD for the same data set. In Fig.4.13 the PSDs are plotted together.

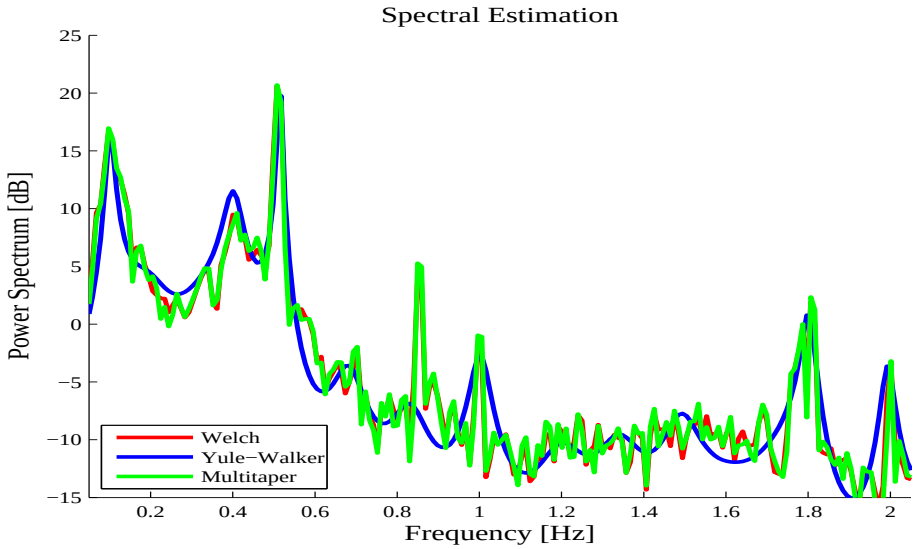

Figure 4.13: Spectral Estimates, 10min of data from Tampere's PMU.

The main argument for using the Multitaper over the Welch is that there is less spectral leakage for spectra having very high dynamic ranges. However, we do not have very high dynamic ranges and so the estimators can be expected to have similar performance and as we can see the nonparametric estimators give very similar estimates, all the major peaks are more or less identical.

The Yule-Walker estimator has some major drawbacks, for poor quality data (see Section 4.4) the estimators will perform poorly. This can be understood by looking at a 12 hour PSD that suffer from these issues, such as the PSD shown in Fig.4.14.

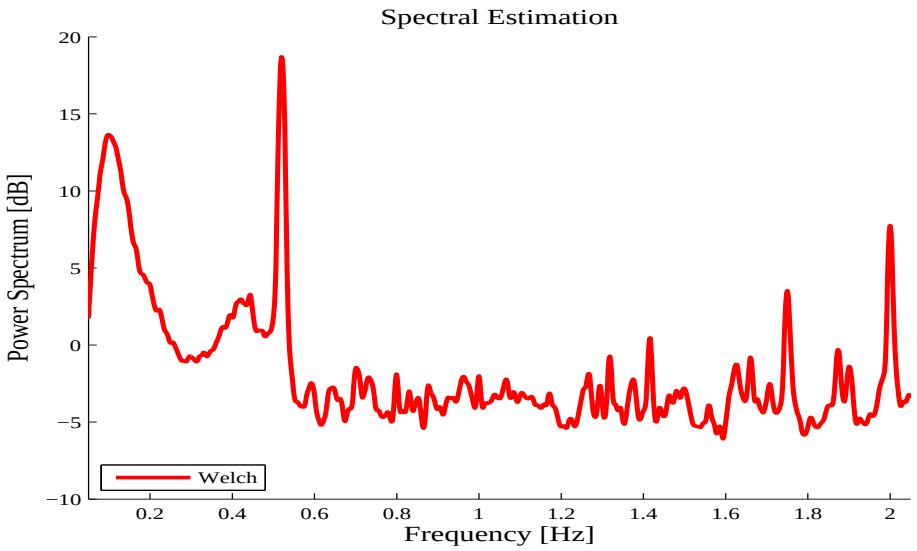

Figure 4.14: PSD computed with 12h of data from LTUs PMU.

The Yule-Walker will obviously not perform well for this data, the estimator will indicate that there are modes all over the frequency range. Also peaks that are to close to each other, see $\sim$1.8 Hz modes in Fig.4.7-4.12, will be compressed. Small mode frequency fluctuations that can be seen in the Welch and Multitaper spectrograms can not be seen in the Yule-Walker spectrogram and peaks are sometimes not at the correct frequency. It can therefore be concluded that the Yule-Walker spectral estimator should not be used on data suffering from the described quality issues, or data that has minor modes close to each other.

The estimator have still been used to compute PSDs later on in this Chapter, but it should be pointed out that this has been done only to illustrate the problems described above and that these estimates have not been used to make any conclusions about the electromechanical modes in the system.

4.6 Results - Computed Spectrograms for Synchrophasors in the Nordic Grid

In this section spectrograms using 72 h of data were computed with the spectral estimators described previously.

A summary of the results follows:

For the PMU located at Tampere:

- 4.15 - Welch Spectral Estimate, 12h of data from Tampere's PMU, 10min PSDs and 8 tapers and 500 samples block size.
- 4.16 - Multitaper Spectral Estimate, 12h of data from Tampere's PMU, 10min PSDs and 8 tapers.
- 4.17 - Yule-Walker Spectral Estimate, 12h of data from Tampere's PMU, 10min PSDs and model order 38.

For the PMU located at LTH:

- 4.18 - Welch Spectral Estimate, 12h of data from LTH PMU, 10min PSDs and 8 tapers and 500 samples block size.
- 4.19 - Multitaper Spectral Estimate, 12h of data from LTH PMU, 10min PSDs and 8 tapers.
- 4.20 - Yule-Walker Spectral Estimate, 12h of data from LTH PMU, 10min PSDs and model order 38.

For the PMU located at LTU:

- 4.21 - Welch Spectral Estimate, 12h of data from LTU PMU, 10min PSDs and 8 tapers and 500 samples block size.
- 4.22 - Multitaper Spectral Estimate, 12h of data from LTU PMU, 10min PSDs and 8 tapers.
- 4.23 - Yule-Walker Spectral Estimate, 12h of data from LTU PMU, 10min PSDs and model order 38.

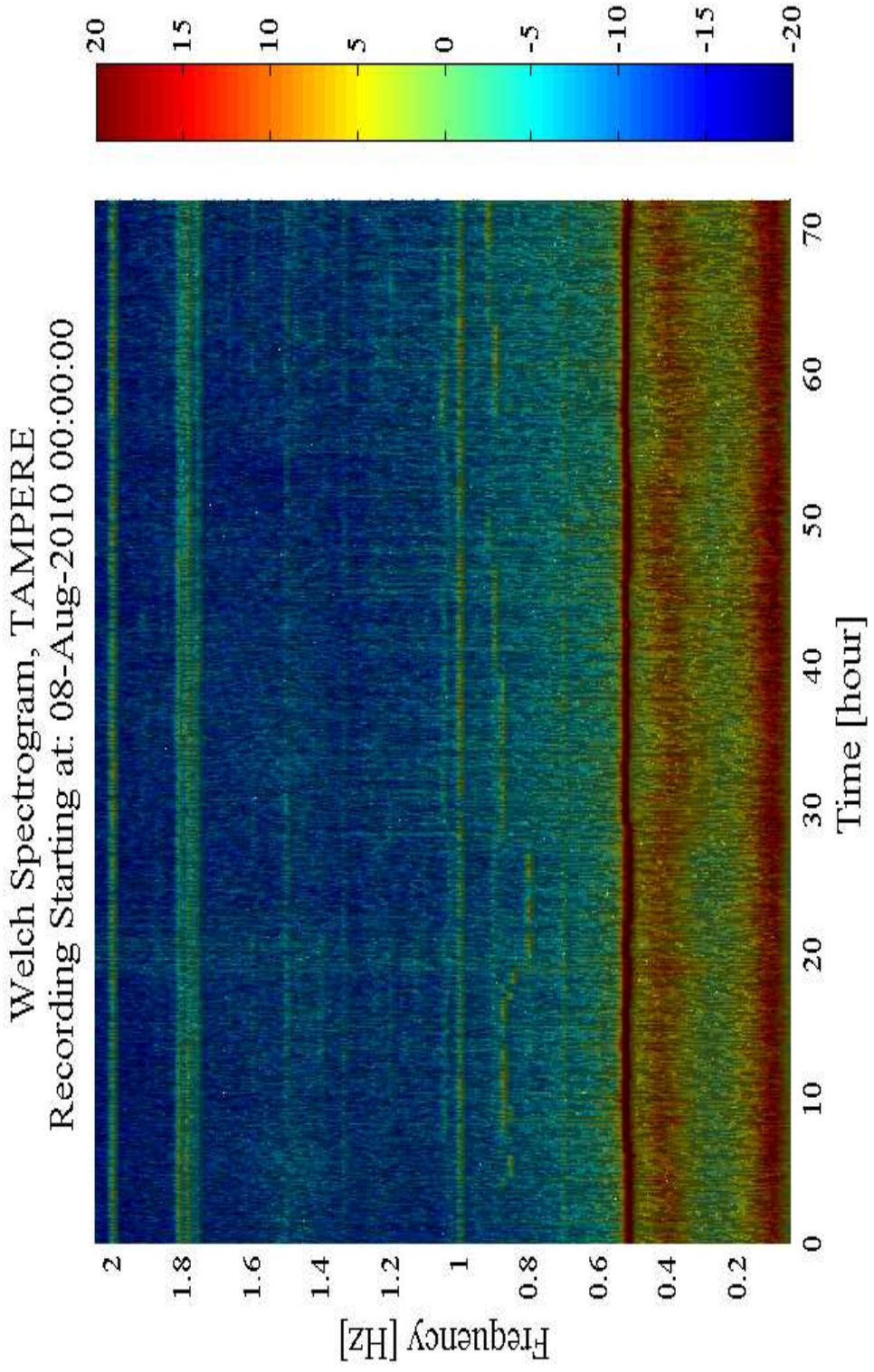

Figure 4.15: Welch Spectral Estimate, 12h of data from Tampere's PMU, 10min PSDs and 8 tapers and 500 samples block size.

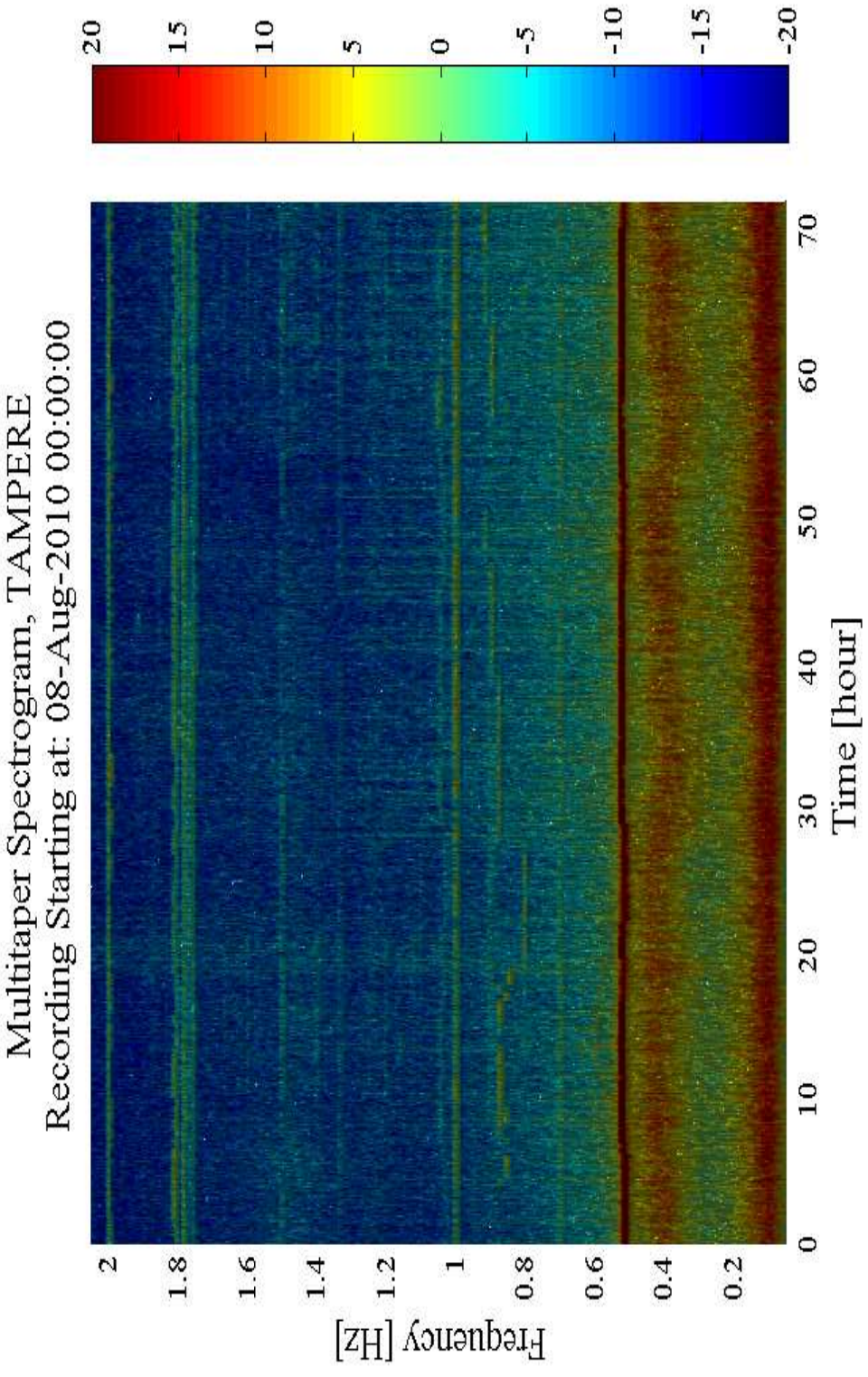

Figure 4.16: Multitaper Spectral Estimate, 12h of data from Tampere's PMU, 10min PSDs and 8 tapers.

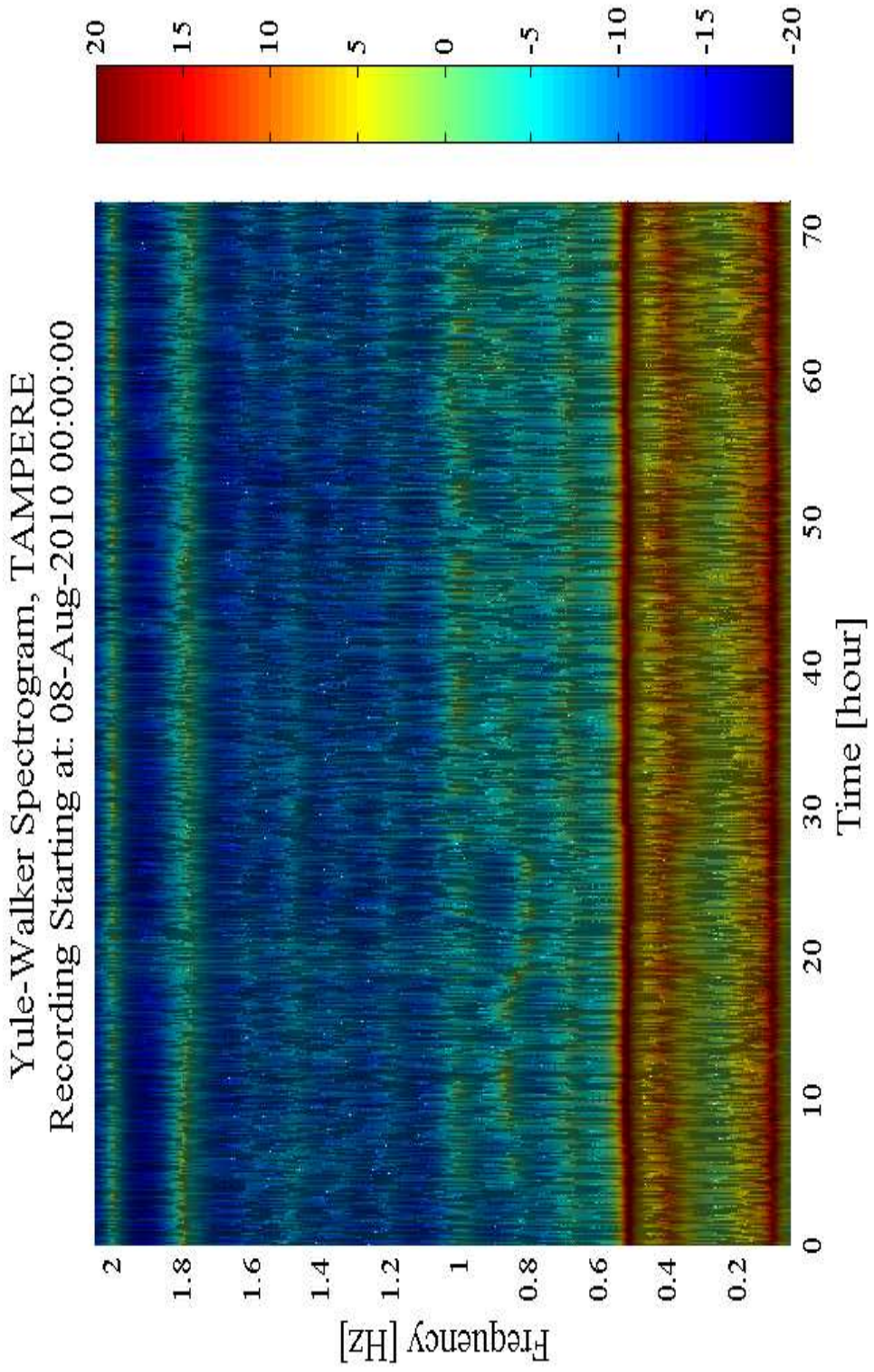

Figure 4.17: Yule-Walker Spectral Estimate, 12h of data from Tampere's PMU, 10min PSDs and model order 38.

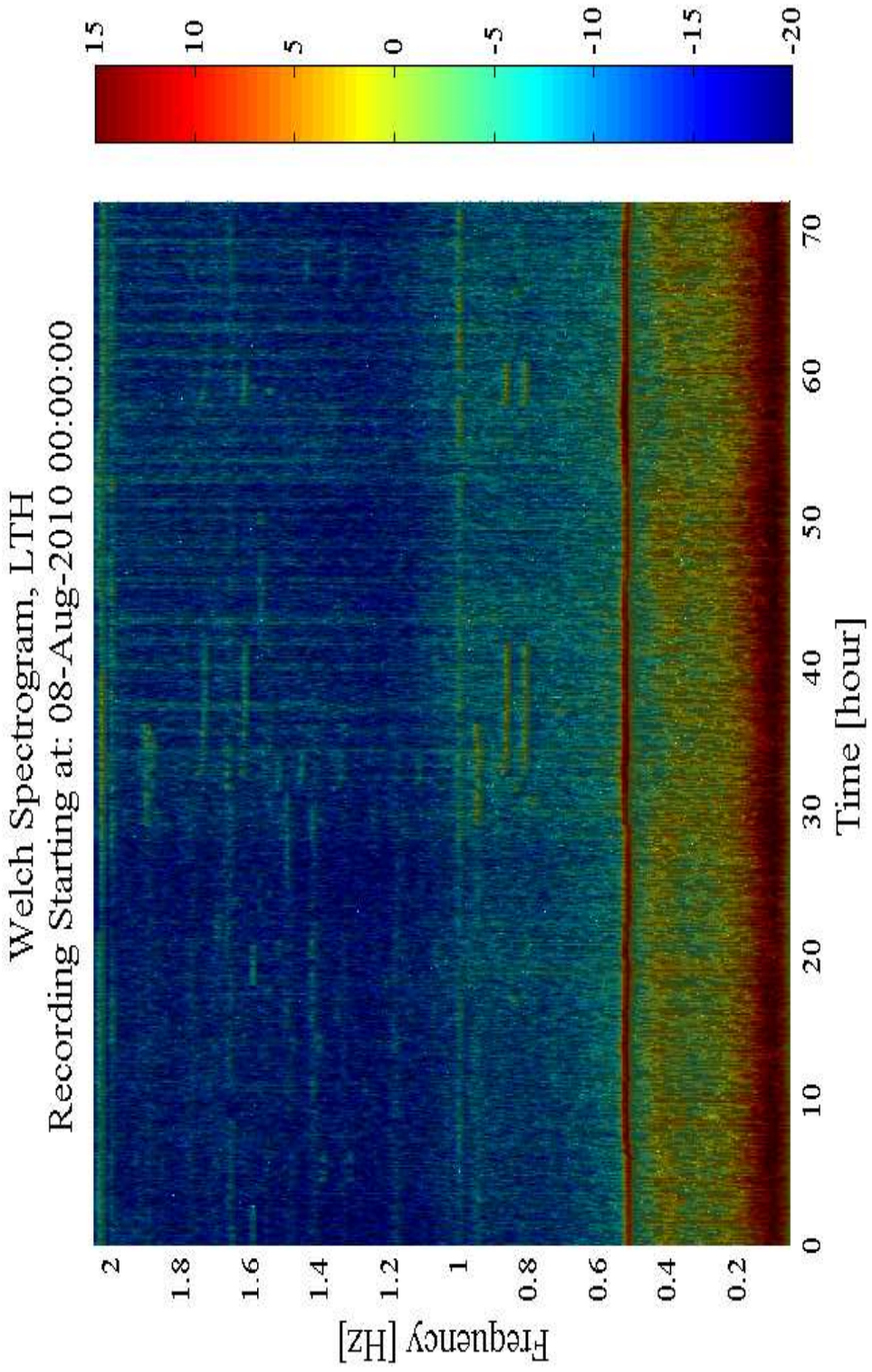

Figure 4.18: Welch Spectral Estimate, 12h of data from LTH PMU, 10min PSDs and 8 tapers and 500 samples block size.

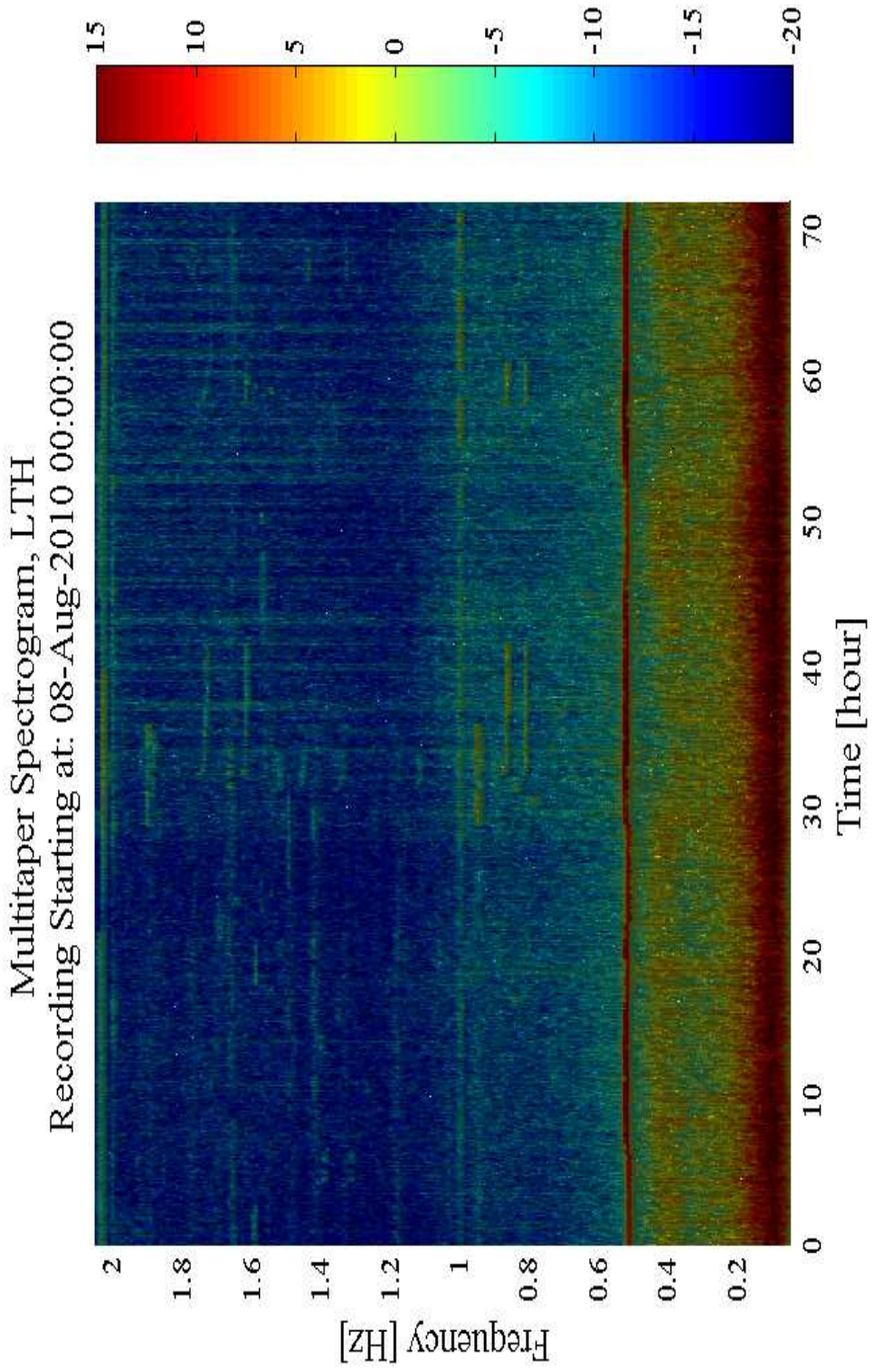

Figure 4.19: Multitaper Spectral Estimate, 12h of data from LTH PMU, 10min PSDs and 8 tapers.

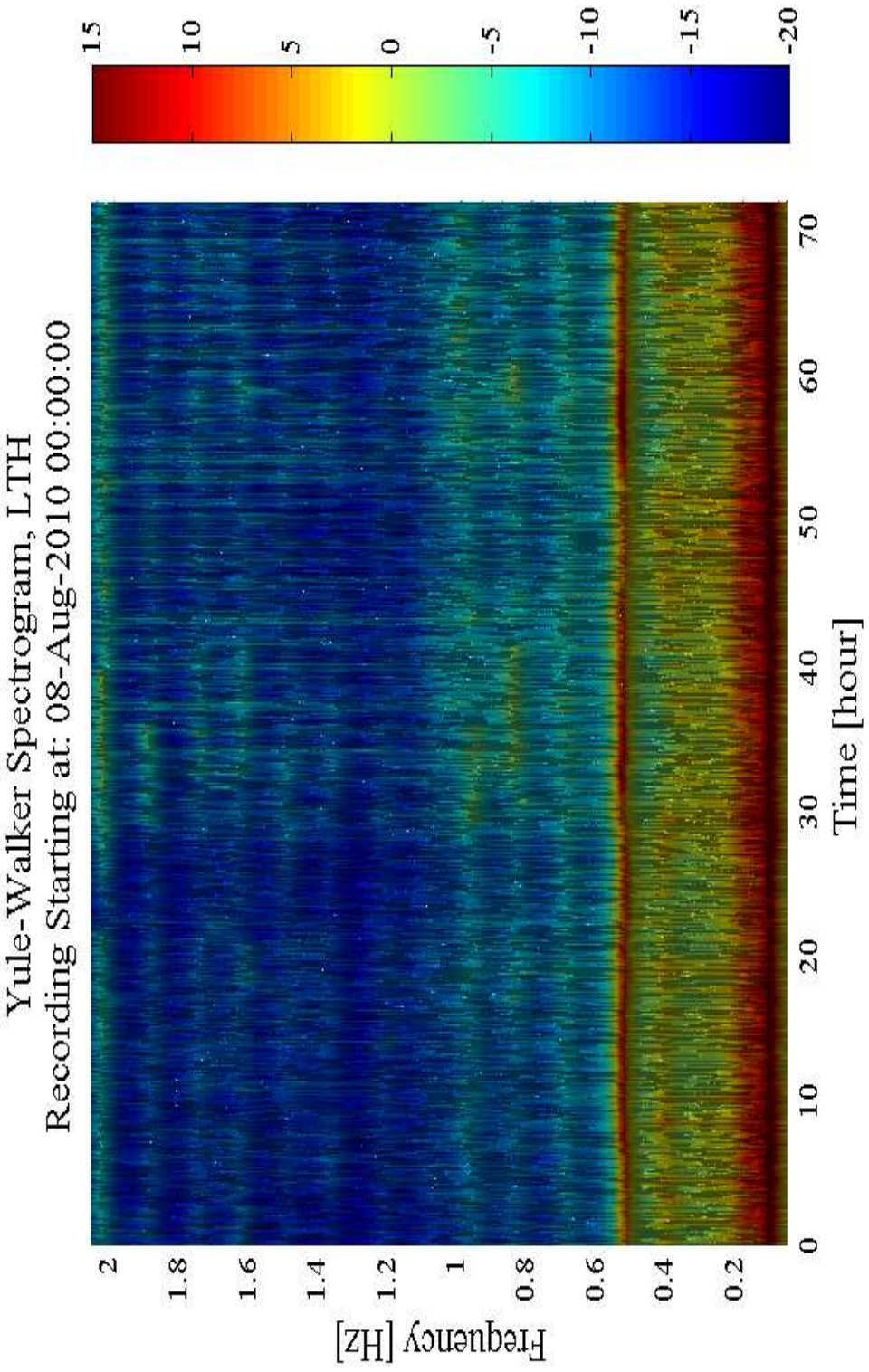

Figure 4.20: Yule-Walker Spectral Estimate, 12h of data from LTH PMU, 10min PSDs and model order 38.

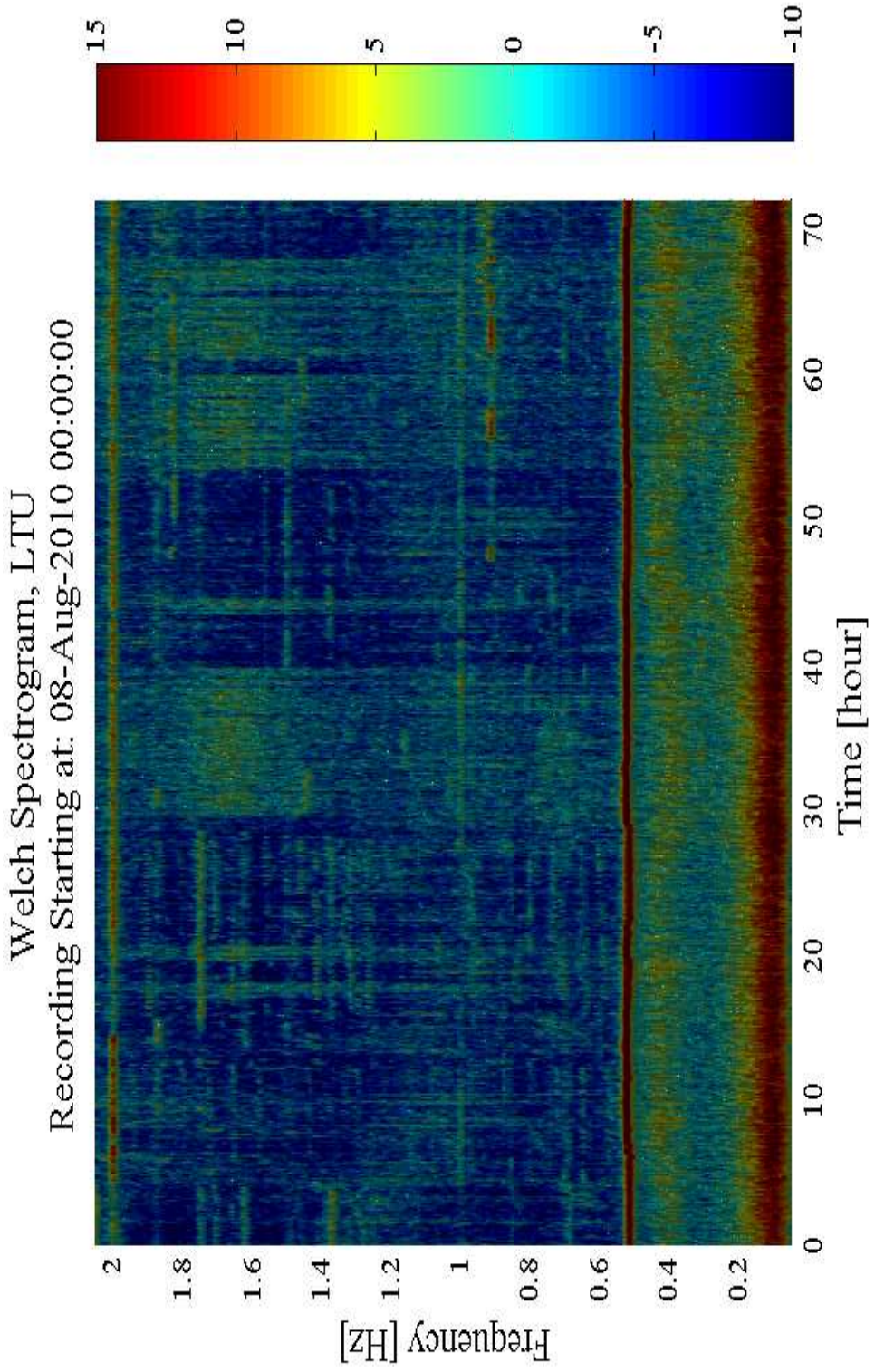

Figure 4.21: Welch Spectral Estimate, 12h of data from LTU PMU, 10min PSDs and 8 tapers and 500 samples block size.

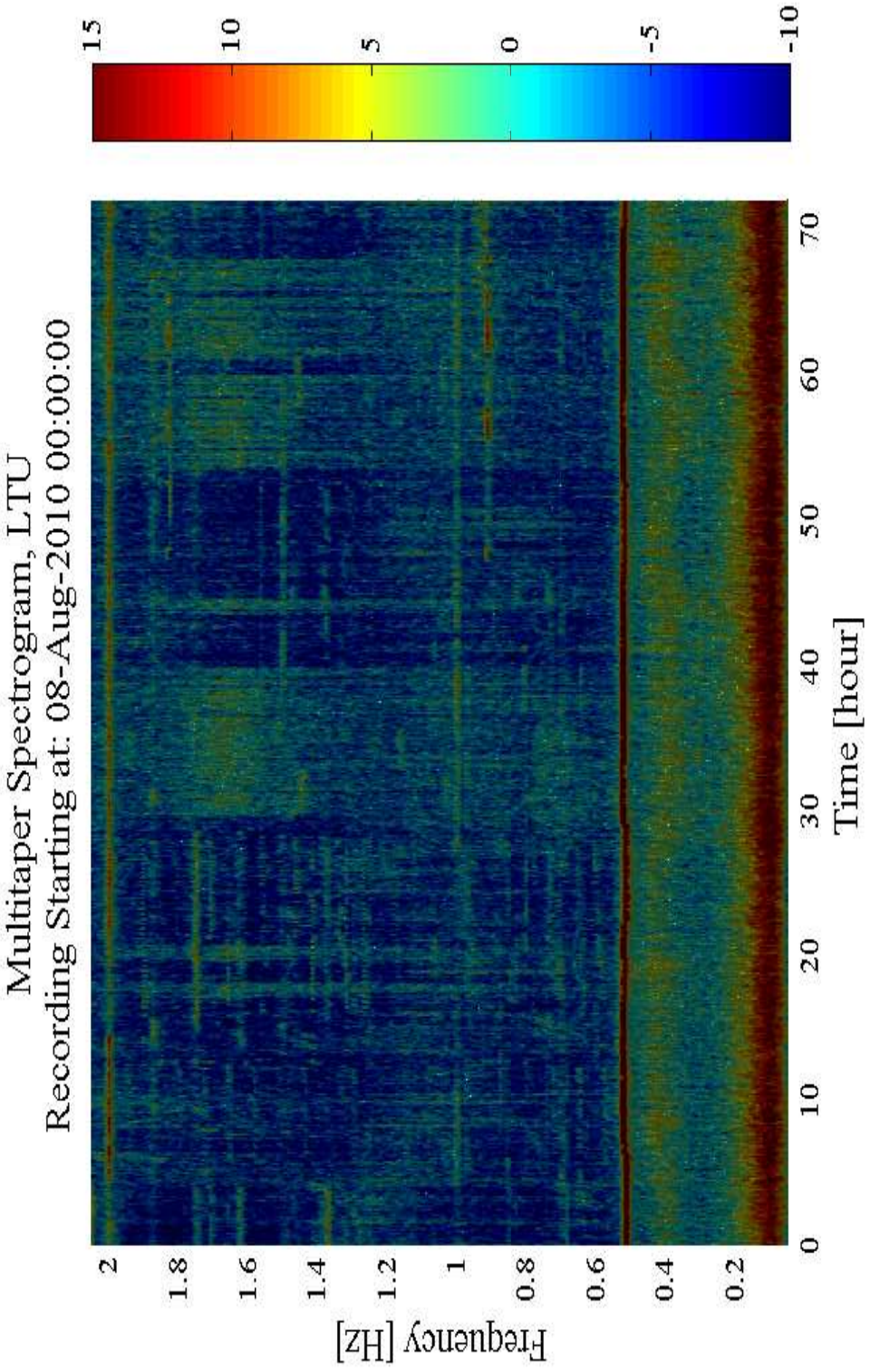

Figure 4.22: Multitaper Spectral Estimate, 12h of data from LTU PMU, 10min PSDs and 8 tapers.

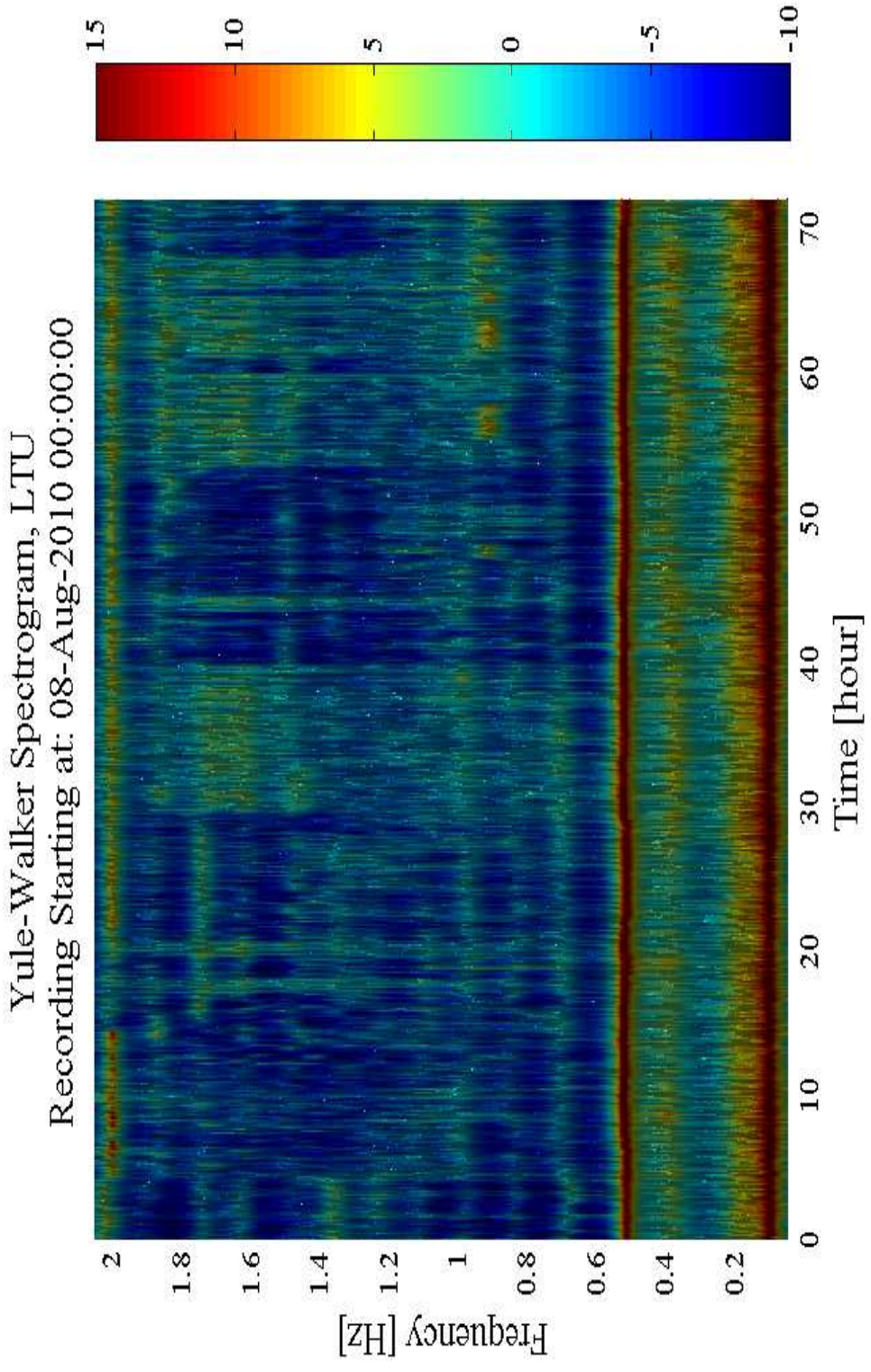

Figure 4.23: Yule-Walker Spectral Estimate, 12h of data from LTU PMU, 10min PSDs and model order 38.

4.7 Location of the Electromechanical Modes

By inspecting FFTs we can separate forced oscillations from electromechanical modes and determine the mode locations. Fig.4.24 illustrated the difference between a mode and a sinusoid in a FFT. The sinusoid has all its spectral content concentrated in one small frequency bin while the modes spectral content is spread around the main peak.

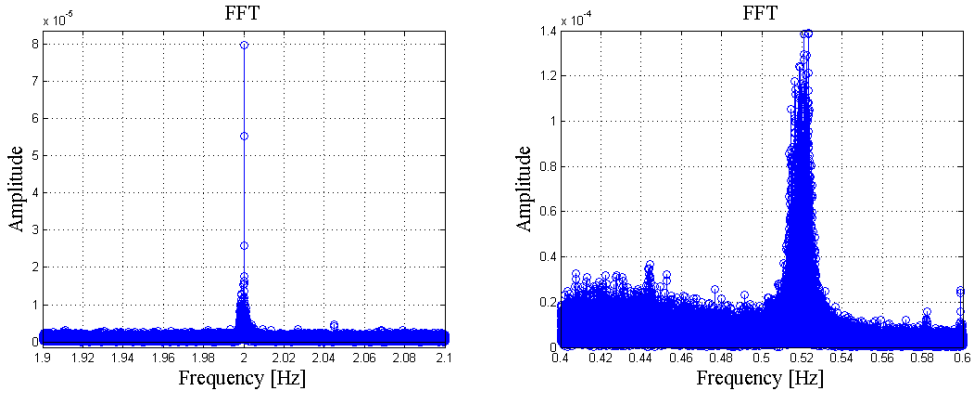

(a) (b)

Figure 4.24: FFT computed with data from Tampere showing (a) Sinusoid (b) Electromechanical mode

After careful inspection of FFTs computed with data from LTH, LTU and Tampere the modes in Table.4.2 were found.

TAMPERE	LTH	LTU
0.08789-0.1172	0.0879-0.1172	0.09766-0.1074
0.3711-0.4395	0.3906-0.4492	0.3711-0.4492
0.5176-0.5273	0.5176-0.5273	0.5176-0.5273
0.6934-0.7324	0.8095-0.8115	0.7031-0.7324
0.8008-0.918	0.8675-0.8685	0.9082-0.9473
1.748-1.758	0.9473-0.9515	
1.776-1.789		
1.807-1.816		

Table 4.2: Mode frequencies from FFTs.

4.8 Inter-area Modes

From Table 4.2 it can be seen that there appears to be three inter-area modes in common to all measurement locations. The first mode is remains of the system frequency control that has not been entirely attenuated, this gives that the main inter-area modes of the system are those in Table 4.3

TAMPERE	LTH	LTU
0.3711-0.4395	0.3906-0.4492	0.3711-0.4492
0.5176-0.5273	0.5176-0.5273	0.5176-0.5273

Table 4.3: Main inter-area modes of the system.

There is one more possible inter-area mode, this mode can only be observed at LTU and Tampere and its frequency is given in Table 4.4.

TAMPERE	LTU
0.6934-0.7324	0.7031-0.7324

Table 4.4: Mode frequency of a possible inter-area mode.

4.9 Pop-ups in the Inter-area Frequency Range

There are a lot of changes in the system dynamics in the frequency range 0.6-1 Hz, modes appear for a few hours only to later disappear. These modes might be the result of local generating units being started and then turned off, or they may be caused by a brief connection to another power system thru a HVDC link, the frequencies of these modes are given in Table.4.5.

For the measurements from LTH pop-ups can be observed between approximately 30-40h and around 60h in Fig.4.18-4.19 and for LTH it can be observed between approximately 50-70h in Fig.4.21-4.22. In the measurements from Tampere there is a pop-up mode that is rather consistent in Fig.4.15-4.16, but there is a lot of change in the frequency of this mode. Similar behavior has been observed in [21] where it was caused by synchronization and separation of interconnected systems.

TAMPERE	LTH	LTU
0.8008-0.918	0.8095-0.8115	0.9082-0.9473
	0.8675-0.8685	
	0.9473-0.9515	

Table 4.5: Mode pop-ups in the inter-area range.

4.10 Conclusions

As concluded in Section 4.5 the Welch and the Multitaper spectral estimators give more or less identical estimates that can be used to monitor frequencies of the electromechanical oscillations in power system. The Yule-Walker on the other hand should not be used for this purpose since the estimator does not provide reliable estimates. To further improve the quality of the estimates one need to find ways to detect and remove the forced oscillations from the measurements.

Chapter 5

Mode Damping Estimation

There exists many different methods for mode damping estimation, most of them require a mathematical model of the system. From such a model the complex eigenvalues $\lambda_i = \sigma_i \pm j\omega_i$ of the modes can be obtained and the damping ratio (or rate of decay) of the oscillation amplitudes can the be calculated as

$$\zeta_i = \frac{-\sigma_i}{\sqrt{\sigma_i^2 + \omega_i^2}} \tag{5.1}$$

However, the process of constructing a highly detailed model of a complex system, such as a power system, can be very time consuming, and if not done in sufficient detail, may still yield unsatisfactory results.

Another approach that is frequently used for damping estimates is to fit a transient (or ringdown) to a simple function on the form

$$\hat{y}(t) = \sum_{i=1}^{P} R_i e^{\lambda_i t} \tag{5.2}$$

the eigenvalues, λ_i, are obtained and the damping can be computed with equation (5.1). This kind of methods have limitations, not only because they depend on the existence of transients in the data, but also depend on sufficient excitation of the modes of interest.

In this Chapter a simple mathematical model, the autoregressive Yule-Walker model, is derived and used for damping estimation. The half-power point method, which estimates the damping from the width of the mode peaks, is also used to compute damping estimates. Both of these methods have been applied to PMU and simulated ambient data to evaluate their performance.

5.1 The Autoregressive Yule-Walker Model

The damping ratio of a mode can be extracted from the autoregressive Yule-Walker model. The model coefficients are the poles corresponding to the the pole polynomial coefficients of an input-output transfer function. And the innovation variance corresponds to the numerator of this transfer function, hence the input/output transfer function is given by

$$H(s) = \frac{\sigma_p}{\sum_{i=1}^{p}(s - \phi_{i,p})} \tag{5.3}$$

Using (4.5) the mode frequencies and corresponding damping ratios can be calculated from the poles (eigenvalues) of the transfer function as follows:

$$\lambda_i = \sigma_i \pm j\omega_i = \Re\{\phi_{i,p}\} \pm \Im\{\phi_{i,p}\} \tag{5.4}$$

$$f_i = \frac{\omega_i}{2\pi} = \frac{\Im\{\phi_{i,p}\}}{2\pi} \tag{5.5}$$

$$\zeta_i = \frac{-\sigma_i}{\sqrt{\sigma_i^2 + \omega_i^2}} = \frac{-\Re\{\phi_{i,p}\}}{\sqrt{\Re\{\phi_{i,p}\}^2 + \Im\{\phi_{i,p}\}^2}} \tag{5.6}$$

Hence, to determine mode frequencies, it is first necessary to obtain a Yule-Walker model. In the next section a method to determine the Yule-Walker autoregressive model order is described.

5.2 Determination of the Yule-Walker Model Order from Partial Autocorrelation Coefficients

An autoregressive process of order p can be described by the model

$$Y_t = \phi_{1,p}Y_{t-1} + \phi_{2,p}Y_{t-2} + ... + \phi_{p,p}Y_{t-p} + \epsilon_t \tag{5.7}$$

where Y_t is zero mean stationary process and $\phi_{1,p}, \phi_{2,p}, .., \phi_{p,p}$ are the model coefficients, ϵ_t is a white noise process with zero mean and variance σ_p^2.

Partial autocorrelation coefficient $\phi_{k,k}$ indicate time dependence between Y_t and Y_{t-k}. For a model order k that is lower or equal to the true model order p we will, as can be seen by the model (5.7), have a time dependence between Y_t and Y_{t-k}, so $\phi_{k,k}$ will be non zero. But if the model order k is higher than p we will have no dependence, and so, $\phi_{k,k}$ will be zero.

With this knowledge it follows that we should be able to determine an appropriate model order by examining $\phi_{k,k}$ for different k and see when it goes from non zero to zero. The problem with this approach is that the estimates $\hat{\phi}_{k,k}$ for different values of $k > p$ wont be zero but will be independently distributed with a zero mean and a variance of approximately $1/N$. The cutoff between $k \leq p$ and $k > p$ might therefore not be that apparent, see Fig 5.1 below.

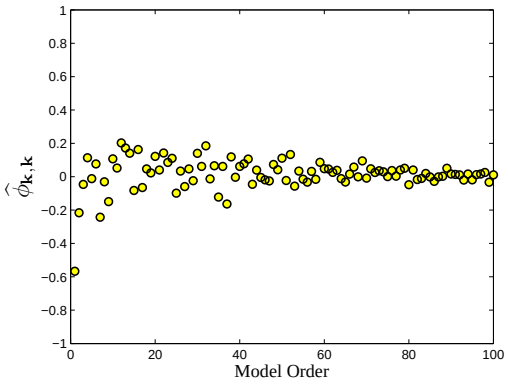

Figure 5.1: $\hat{\phi}_{k,k}$ vs. model order for a 3000 sample estimate, no apparent cutoff.

In order to visualize a cutoff the variance of $\hat{\phi}_{k,k}$ for $k > p$ has to be reduced somehow, this is done by computing $\hat{\phi}_{k,k}$ for different data sequences of the same process and then taking the minimum value of $\hat{\phi}_{k,k}$ for each k. By doing this $\hat{\phi}_{k,k}$ will for $k \leq p$ be relatively unaffected while for $k > p$ $\hat{\phi}_{k,k}$ will move towards zero. Furthermore the absolute value of each $\hat{\phi}_{k,k}$ is taken to make the cutoff more visually apparent in the plots.

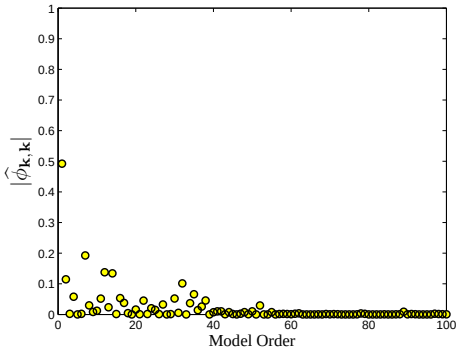

Figure 5.2: LTU, $|\hat{\phi}_{k,k}|$ vs. model order for 12h of data and 3000 samples per estimate. Indicates that a model of order 38 should be used.

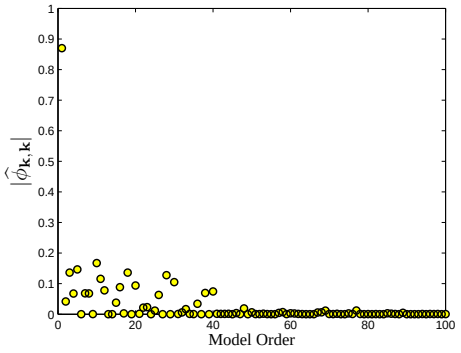

Figure 5.3: LTH, $|\hat{\phi}_{k,k}|$ vs. model order for 12h of data and 3000 samples per estimate. Indicates that a model of order 40 should be used.

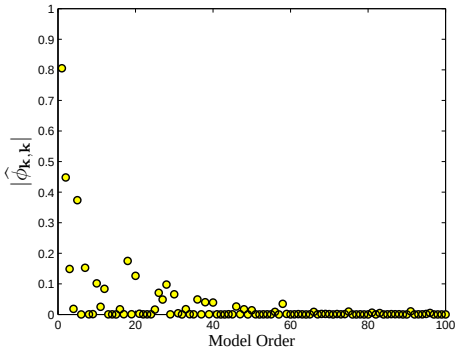

Figure 5.4: Tampere, $|\hat{\phi}_{k,k}|$ vs. model order for 12h of data and 3000 samples per estimate. Indicates that a model of order 40 should be used.

5.3 Half-Power Point Method

By examining the peak width of a mode the damping can be approximated, a narrow peak means a low damped mode while a wide peak means that the mode is well damped. The half-power point method states that the distance[1] between the two half-power points surrounding the peak center is roughly proportional to the mode damping[2].

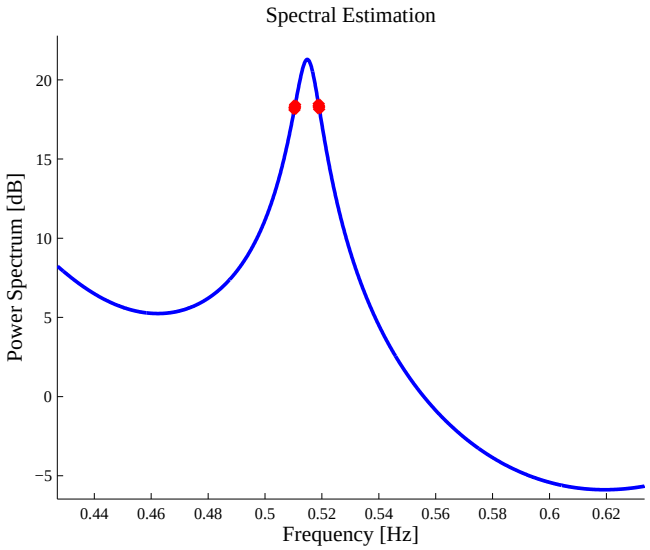

Figure 5.5: Illustration of the half-power point method were the half-power points are marked with red dots.

The method is based of the assumption that the frequency response of the system can be modeled as:

$$|H(\omega)| = \frac{1}{\sqrt{(1-(\frac{\omega}{\omega_n})^2)^2 + (2\zeta\frac{\omega}{\omega_n})^2}} \tag{5.8}$$

A mode will thus appear at the frequency $\omega = \omega_n$ and the damping of this mode can be derived from the equation above yielding:

$$\zeta = \frac{\omega_2 - \omega_1}{2\omega_n} \tag{5.9}$$

were $|H(\omega_1)| = |H(\omega_2)| = \frac{1}{\sqrt{2}}|H(\omega_n)|$.

[1] This distance is given by $\omega_2 - \omega_1$.

[2] PSDs from the Welch spectral estimator are used to compute the half-power point damping estimates in this Chapter.

5.4 Simulations

To verify that the methods used for damping estimation perform correctly the system from Section 4.3 is again used, the difference is that here we focus solely on the inter-area mode.

Frequency (Hz)	Damping (%)
0.8328	6.93

Table 5.1: Mode frequency and damping of the inter-area mode from the simulated system.

For 12 hours of simulated data the methods give, using 10 min blocks, the following estimates

Method	$\overline{f}$ (Hz)	$\overline{\zeta}$ (%)	Variance
Yule-Walker	0.8342	6.5826	0.3564
Half-Power Point Method	0.8324	6.7714	0.4215

Table 5.2: Mode frequency, damping and variance from the methods.

From the Table 5.2 it can be seen that both methods give decent damping estimates. It is remarkable that the methods give almost identical estimates, this is shown in Fig.5.6 and Fig.5.7 where the variation in damping for the whole 12 hour period have been plotted.

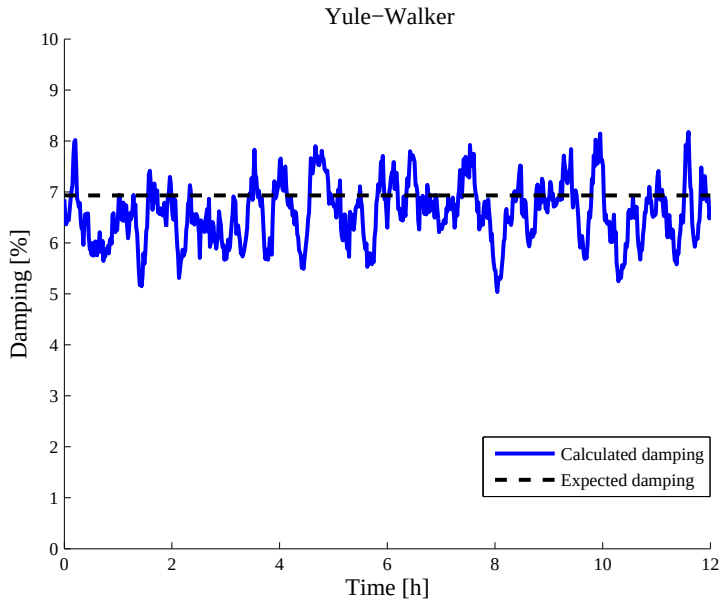

Figure 5.6: Damping estimates from the Yule-Walker model, 10 min blocks of data, black dotted line showing expected damping.

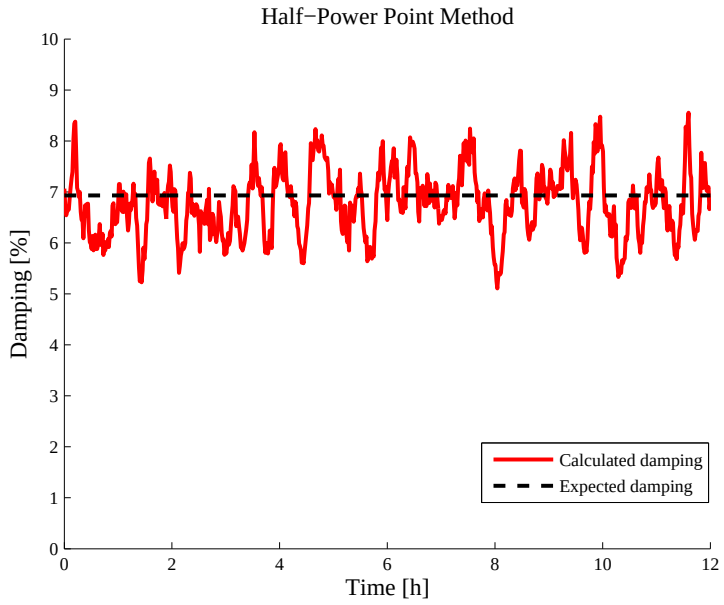

Figure 5.7: Damping estimates from the half-power point method, 10 min blocks of data, black dotted line showing expected damping.

5.5 Effect of Forced Oscillations and Undamped Sinusoids.

Forced oscillations and undamped sinusoids (see section 4.4) will, if superimposed over a system mode, have negative effects when computing accurate damping estimates. By computing the FFT of a damped sinusoid before and after an undamped sinusoid with the same frequency has been added, it can be seen how the performance of the half-power point method is affected by the undamped sinusoid.

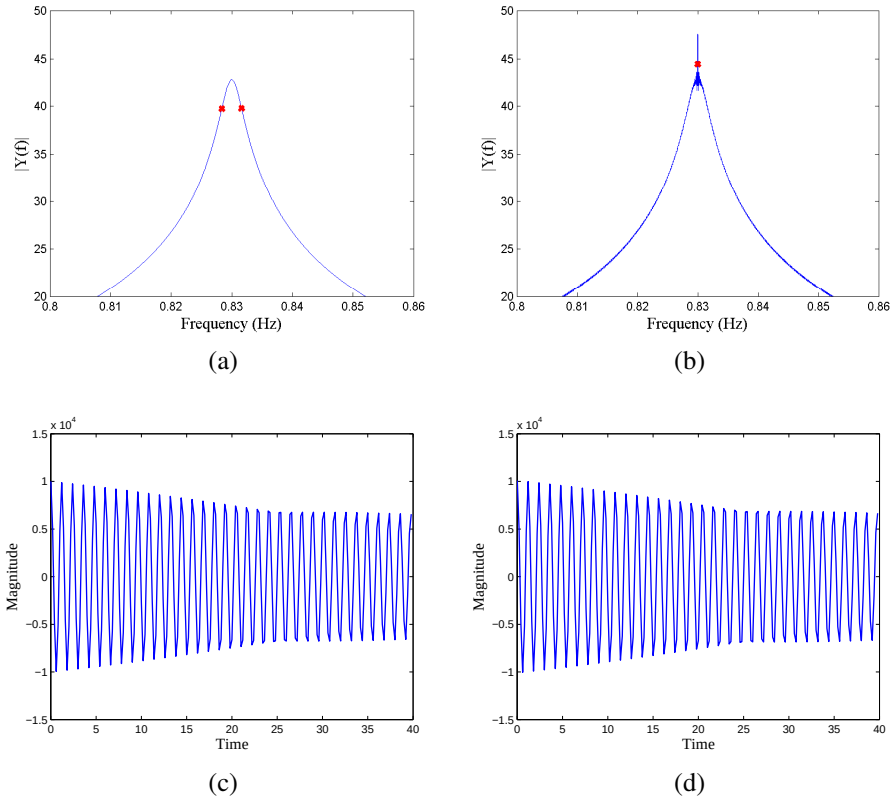

Figure 5.8: The half power points for (a) damped sinusoid (b) damped sinusoid with an superimposed undamped sinusoid, (c) and (d) show the corresponding time domain signals.

From Fig.5.8 it can be seen that an undamped sinusoid with only 1 percent of the magnitude of the original sinusoid will have a huge impact on the damping estimates obtained. The half-power points will be very close together and equation (5.8) will give a much to small damping ratio.

For the Yule-Walker AR model, the undamped sinusoid will decrease the real part of the eigenvalues, while the imaginary part will be relatively unaffected, and so equation (5.6) will also yield too small damping ratios.

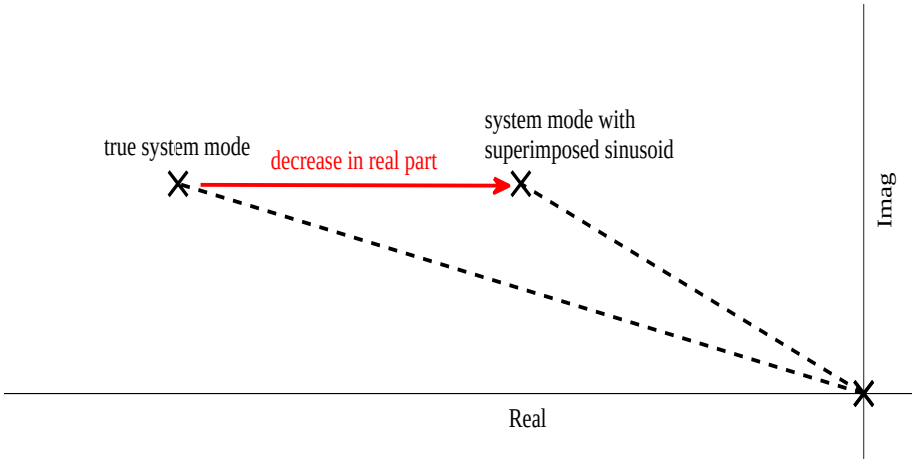

Figure 5.9: Effect of a superimposed sinusoid on the eigenvalue of a system mode.

Of course, often the sinusoids will not be directly superimposed over the mode, but rather located in the nearby frequency region. In those cases both methods will have difficulties, the sinusoid peak may be mistaken for the mode peak. If located very close to the mode peak, the sinusoid will cause the width of the peak of the true mode to grow. In both cases the damping estimates will be severely affected.

5.6 Results

In this section the damping estimates obtained with the two methods discussed previously are documented.

0.5 Hz Mode

Method	$\overline{f}$ (Hz)	$\overline{\zeta}$ (%)	Variance
Yule-Walker	0.5181	0.7413	0.0257
Half-Power Point Method	0.5174	0.7096	0.0049

Table 5.3: Tampere, mode frequency, damping and variance from both methods.

Method	$\overline{f}$ (Hz)	$\overline{\zeta}$ (%)	Variance
Yule-Walker	0.5190	1.8665	0.1739
Half-Power Point Method	0.5174	0.7108	0.0049

Table 5.4: LTH, mode frequency, damping and variance from both methods.

Method	$\overline{f}$ (Hz)	$\overline{\zeta}$ (%)	Variance
Yule-Walker	0.5177	1.0286	0.0553
Half-Power Point Method	0.5174	0.7078	0.0047

Table 5.5: LTU, mode frequency, damping and variance from both methods.

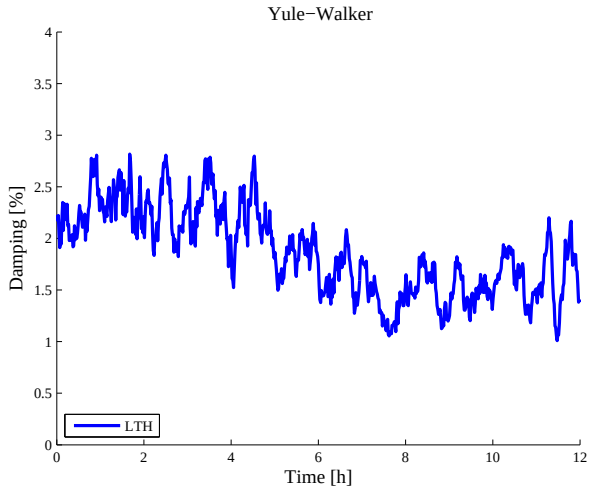

(a)

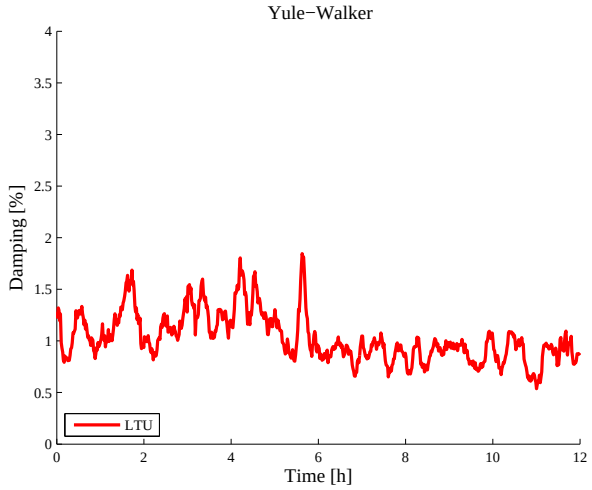

(b)

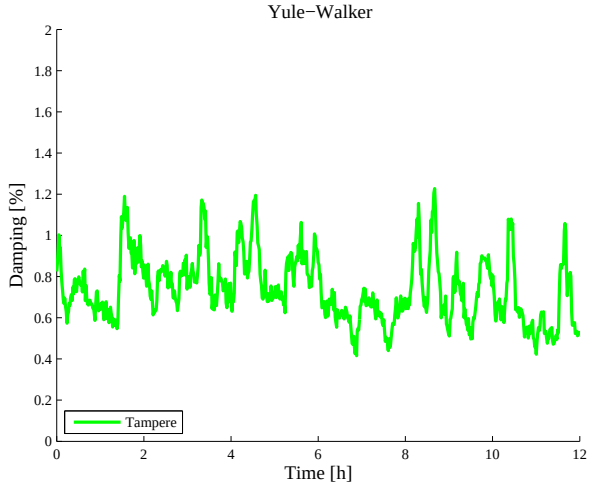

(c)

Figure 5.10: Damping estimates, Yule-Walker, 10 min of data for each estimate, from (a) LTH (b) LTU (c) Tampere

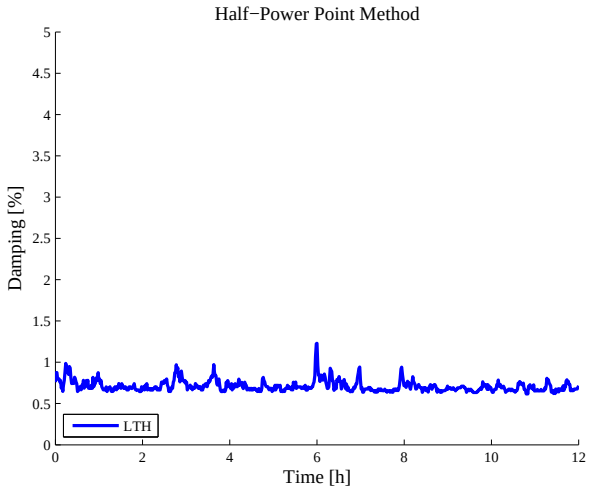

(a)

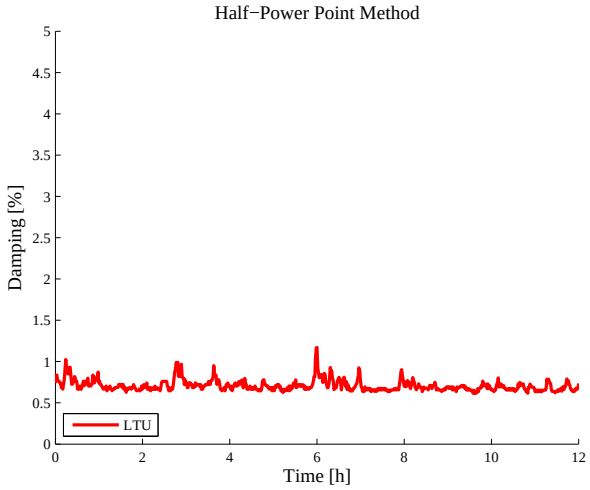

(b)

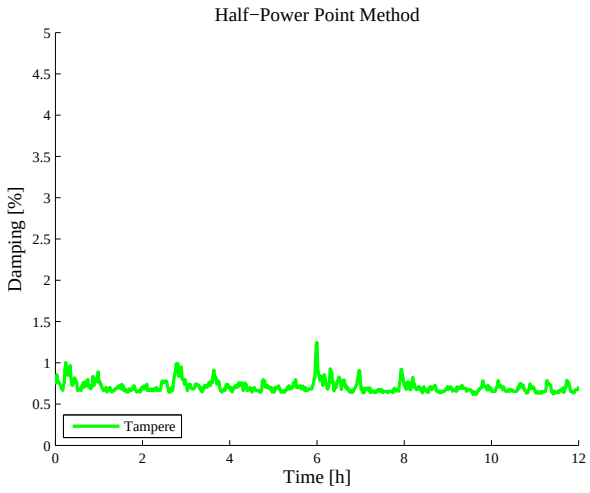

(c)

Figure 5.11: Damping estimates, half-power point method, 10 min of data for each estimate, from (a) LTH (b) LTU (c) Tampere

0.4 Hz Mode

Method	$\overline{f}$ (Hz)	$\overline{\zeta}$ (%)	Variance
Yule-Walker	0.4079	7.2395	2.0405
Half-Power Point Method	0.4130	9.5469	8.2036

Table 5.6: Tampere, mode frequency, damping and variance from both methods.

Method	$\overline{f}$ (Hz)	$\overline{\zeta}$ (%)	Variance
Yule-Walker	0.4023	8.2929	2.2361
Half-Power Point Method	0.4052	11.1226	11.7186

Table 5.7: LTH, mode frequency, damping and variance from both methods.

Method	$\overline{f}$ (Hz)	$\overline{\zeta}$ (%)	Variance
Yule-Walker	0.3883	10.0402	4.1682
Half-Power Point Method	0.4122	10.4220	10.0292

Table 5.8: LTU, mode frequency, damping and variance from both methods.

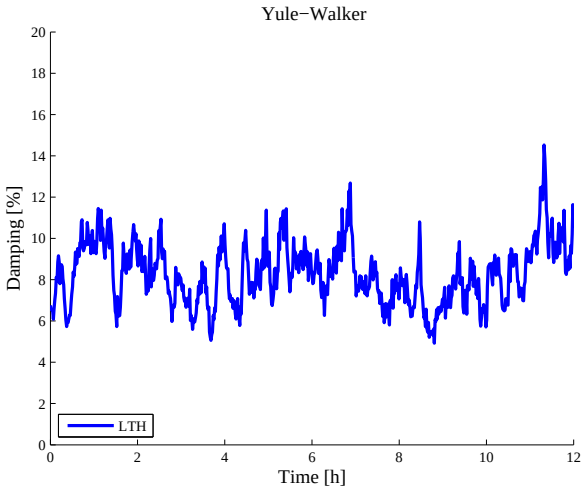

(a)

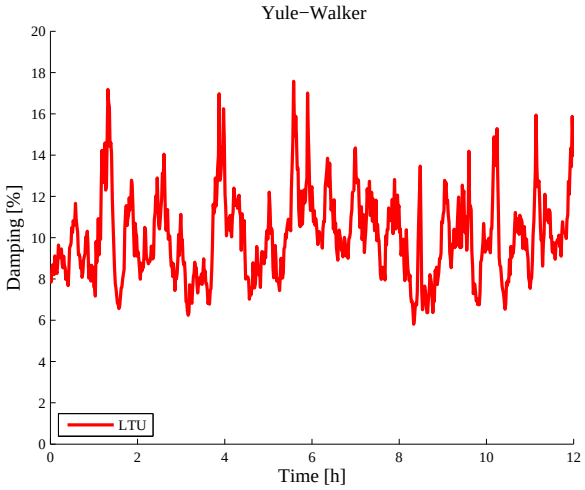

(b)

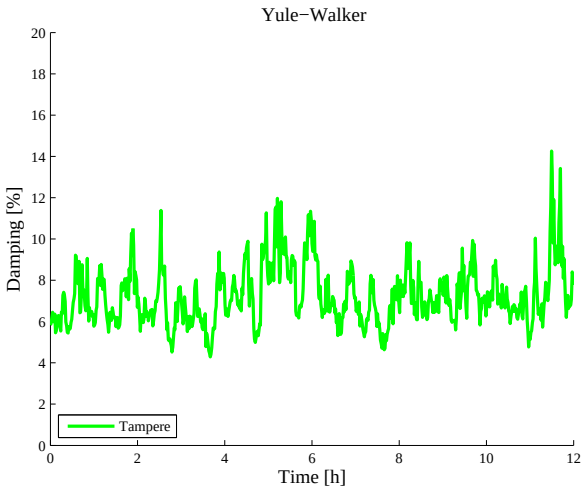

(c)

Figure 5.12: Damping estimates, Yule-Walker, 10 min of data for each estimate, from (a) LTH (b) LTU (c) Tampere

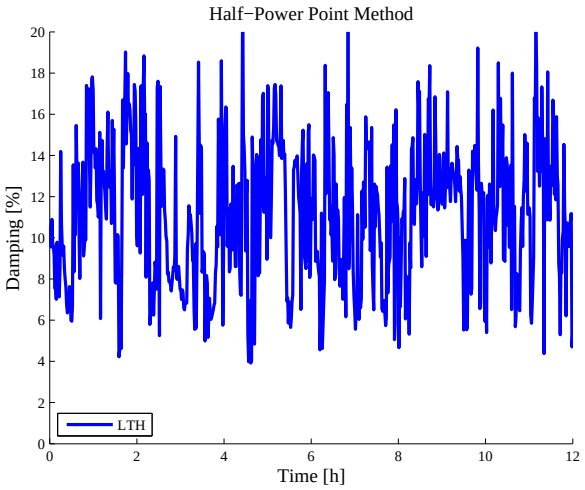

(a)

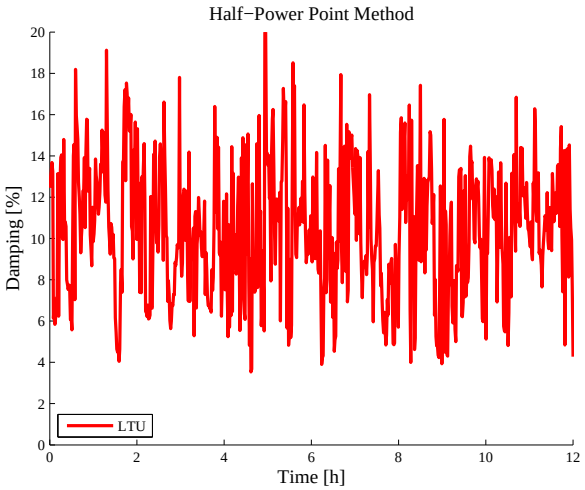

(b)

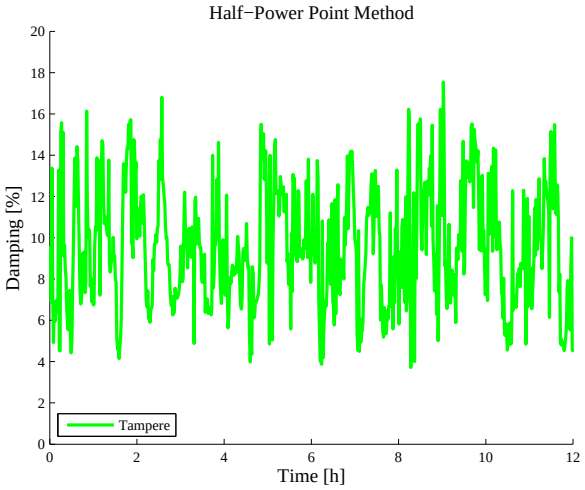

(c)

Figure 5.13: Damping estimates, half-power point method, 1 hour of data for each estimate, from (a) LTH (b) LTU (c) Tampere

5.7 Conclusions

From section 5.4 we can conclude that Yule-Walker and half-power point method work well on simulated data, but when it comes to real PMU data the performance of the methods is not satisfactory. This is of course to be expected, the quality of the PMU data is much degraded due to the presence of forced oscillations, as explained in section 5.5.

The damping estimates for the $\sim$0.5 Hz mode are very low, this is likely because of the existence of a sinusoid at the same frequency as the mode. The variance of the estimates is also very low, this can be explained by the sinusoid, which gives a constant and dominating contribution the the damping estimates.

For the $\sim$0.4 Hz mode there is a lot of variance in the estimates, there is no single sinusoid that completely dominates the frequency region. Even so, the existence of low-amplitude sinusoids in the same region as the modes seems highly likely, in fact inspection of the FFTs in section 4.7 confirm this. This causes problems for both the Yule-Walker and the Half-Power Point Method because these sinusoids may sometimes be mistaken for the peak of the mode or they may cause the peak width to grow, therefore these estimates will be both unreliable and have much variance.

Chapter 6

Conclusions and Future Work

Data from phasor measurement units can be efficiently handled with the developed GUI and associated algorithms, and used to obtain ambient data for spectral analysis. Additional software could be developed to further automate the off-line analysis of phasor measurement data.

The Welch and the Multitaper spectral estimators work equally well when computing spectrograms, these spectrograms have the potential to be used for real-time monitoring of electromechanical oscillations in power systems. Hence, software that could be used to monitor the system also needs to be developed.

To increase the understanding of the electromechanical dynamics of the Nordic power system more measurement locations are needed. By using additional phasor measurement data from Denmark and Norway a much more complete picture of the electromechanical dynamics of the system could be obtained.

To further improve the quality of computed spectrograms and in order to be able to obtain reliable damping estimates, methods that can detect and remove the effect of forced oscillations in the measurements need to be developed. To this aim transient data can be used to evaluate the performance of ambient data algorithm, by comparing estimates between ambient and transient data.

References

[1] J.H. Chow (Ed.), “Time-Scale Modeling of Dynamic Networks with Applications to Power Systems,” New York: Springer-Verlag, 1982.

[2] M. Klein, G. J. Rogers, and P. Kundur, “A Fundamental Study of Inter-Area Oscillations in Power Systems,” *IEEE Transactions on Power Systems,* vol. 6, no. 3, pp. 914-921, Aug. 1991.

[3] A.J.F.Hauer, D.J.Trudnowski, and J.G.DeSteese, “A Perspective on WAMS Analysis Tools for Tracking of Oscillatory Dynamics,” In Proceedings of the IEEE Power Engineering Society General Meeting, June 2007.

[4] John W. Pierre, Ning Zhou, Manu Parashar, Daniel Trudnowski and John Hauer, "Performance of Three Mode-Meter Block Processing Algorithms for Automated Dynamic Stability Assesment", IEEE TRANSACTION ON POWER SYSTEMS, VOL. 23, NO.2, 2008.

[5] A. Phadke and J. Thorp, *Synchronized Phasor Measurements and Their Applications*. New York: Springer, 2008.

[6] L. Vanfretti and J.H. Chow, “Synchrophasor Data Applications for Wide-Area Systems,” Invited Paper — PMU/WAMS Paper Session, In Proceedings of the Power System Computation Conference 2011, August 2011, Stockholm, Sweden.

[7] Teknikredaktörerna AB AB, "The power transmission network in northwestern Europe", $www.svk.se/$, 2003.

[8] Luigi Vanfretti, Luke Dosiek, John W. Pierre, Daniel Trudnowski, Joe H. Chow, Rodrigo García-Valle and Usman Aliyu, "Application of Ambient Analysis Techniques for the Estimation of Electromechanical Oscillations from Measured PMU Data in Four Different Power Systems", European Transactions on Electrical Power, Special Issue on PMU Data and their Applications, 2010.

[9] openPDC, "About the openPDC", $www.openpdc.codeplex.com/$,

[10] openHistorian, $www.openhistorian.codeplex.com/$,

[11] Moustafa Chenine, Luigi Vanfretti, Sebastian Bengtsson and Lars Nordström, "Implementation of an Experimental Wide-Area Monitoring Platform for Development of Synchronized Phasor Measurement Applications", International Implementation Experience and Prospective Applications of Synchrophasors and their Supporting Infrastructures Panel Session, IEEE, 2011.

[12] Robert Almgren, "MySQL and Matlab"
$www.mmf.utoronto.ca/resrchres/mysql/$,

[13] J. H. Chow, L. Vanfretti, *et al*, "Preliminary Synchronized Phasor Data Analysis of Disturbance Events in the US Eastern Interconnection," In Proceedings of the IEEE/PES Power System Conference and Exposition (PSCE) 2009.

[14] North-American Synchro-Phasor Initiative, "Synchro-Phasor Data Validation", *White Paper*, October 2010. Available on-line: http://www.naspi.org

[15] Torkel Glad and Lennart Ljung, "CONTROL THEORY - Multivariate and Nonlinear Methods", TAYLOR and FRANCIS 2000.

[16] Thai-Hoa Le and Yukio Tamura, "MODAL IDENTIFICATION OF AMBIENT VIBRATION STRUCTURE USING FREQUENCY DOMAIN DECOMPOSITION AND WAVELET TRANSFORM", The Seventh Asia-Pacific Conference on Wind Engineering 2009.

[17] David B. Percival and Andrew T. Walden, "SPECTRAL ANALYSIS FOR PHYSICAL APPLICATIONS - Multitaper and Conventional Uniovariate Techniques", Cambridge University Press 1998.

[18] L. Vanfretti, R. García-Valle, K. Uhlen, E. Johansson, D. Trudnowski, J. W. Pierre, J. H. Chow, O. Samuelsson, J. Østergaard, K. E. Martin, "Estimation of Eastern Denmark's Electromechanical Modes from Ambient Phasor Measurement Data", In Proceedings of the IEEE PES General Meeting, 2010.

[19] N. Martins and L. T. G. Lima. "Eigenvalue and frequency domain analysis of small-signal electromechanical stability problems." In IEEE/PES Symposium on Applications of Eigenanalysis and Frequency Domain Methods, 1989.

[20] L. Vanfretti, and J. H. Chow, "Analysis of Power System Oscillations for Developing Synchrophasor Data Applications," In Proceedings 2010 Symposium Bulk Power System Dynamics and Control VIII.

[21] L. Vanfretti, "Real-life examples: México," In Chapter 2, *Modal Identification of Electromechanical Modes*, Juan Sanchéz-Gasca, Mariesa Crow, Daniel Trudnowski, John Pierre and Arturo Messina(Editors), IEEE PES Task Force on Modal Identification of Electromechanical Modes, Special Publication, to be published, 2011.